PARAMETER ESTIMATION IN A STRUCTURAL ACOUSTIC SYSTEM WITH FULLY NONLINEAR COUPLING CONDITIONS [1]

H.T. Banks
Center for Research in Scientific Computation
North Carolina State University
Raleigh, NC 27695

R.C. Smith
Department of Mathematics
Iowa State University
Ames, IA 50011

ABSTRACT

A methodology for estimating physical parameters in a class of structural acoustic systems is presented. The general model under consideration consists of an interior cavity which is separated from an exterior disturbance by an enclosing elastic structure. Piezoceramic patches are bonded to or embedded in the structure; these can be used both as actuators and sensors in applications ranging from the control of interior noise levels to the determination of structural flaws through nondestructive evaluation techniques. The presence and excitation of the patches, however, changes the geometry and material properties of the structure as well as involves unknown patch parameters, thus necessitating the development of parameter estimation techniques which are applicable in this coupled setting. In developing a framework for approximation, parameter estimation and implementation, strong consideration is given to the fact that the input operator is unbonded due to the discrete nature of the patches. Moreover, the model is weakly nonlinear as a result of the coupling mechanism between the structural vibrations and the interior acoustic dynamics. Within this context, an illustrating model is given, well-posedness and approximation results are discussed and an applicable parameter estimation methodology is presented. The scheme is then illustrated through several numerical examples with simulations modeling a variety of commonly used structural acoustic techniques for system excitation and data collection.

[1]The research of H.T.B. was supported in part by the Air Force Office of Scientific Research under grants AFOSR-90-0091 and AFOSR-F49620-93-1-0198. This research was also supported by the National Aeronautics and Space Administration under NASA Contract Numbers NAS1-18605 and NAS1-19480 while H.T.B. was a visiting scientist and R.C.S. was in residence at the Institute for Computer Applications in Science and Engineering (ICASE), NASA Langley Research Center, Hampton, VA 23681.

1 Introduction

The recent success of piezoceramic materials as sensors and actuators in applications involving structural vibrations has spawned intense study into questions regarding the modeling of piezoceramic actuator/sensor interactions with underlying structures, the optimal design, placement and number of actuators/sensors to be used, and the development of effective control strategies in a variety of environments. When bonded to or embedded in a thin structure (beam, plate or shell), piezoceramic patches derive their actuating capacity from the piezelectric property that an induced voltage produces a strain in the material thus leading to the potential for producing in-plane forces and/or moments when the patches are mounted in pairs. Conversely, their sensing capabilities are due to the dual piezoelectric effect; namely, a mechanical deformation leads to the generation of a proportional voltage across the element which can then be used to measure accumulated strain.

However, the bonding or embedding of patches in the underlying structure changes not only the geometry of the structure but also physical properties such as the density, stiffness, Poisson ratio and damping coefficients, when indeed, many of these parameters are unknown even for the homogeneous, uniform host structure material. This necessitates the development of effective parameter identification methods to be used when estimating system parameters in applications such as experimental model validation, the determination of optimal placement and number of patches, the use of piezoceramic patches in nondestructive evaluation (NDE) techniques, and the implementation of model-based control schemes. We point out that the estimation of physical parameters in this setting differs from that considered in much of the previous literature (see [6] and the references therein) in that here the patch contributions to the system lead to unbounded (discontinuous) input and output operators due to the fact that the patches cover only discrete portions of the structure.

Parameter estimation methods for distributed parameter systems involving unbounded operators have been developed and tested in the case in which piezoceramic patches are used as sensors and actuators when bonded to a transversely vibrating beam [15, 16]. There, fit-to-data techniques involving PDE models were developed which could be used to estimate unknown beam parameters given various data forms. Moreover, in that setting, results pertaining to convergence and continuous dependence on data were obtained in a variety of cases involving physically tractable methods for exciting the system and measuring data.

In this work, we develop an analogous methodology which can be used for estimating physical parameters in structural acoustic systems. In the systems of interest, an exterior disturbance (e.g. noise source, mechanical or electromagnetic force) is separated from an interior cavity by a thin elastic structure (a beam, plate or shell). As energy is transferred from the exterior field to the structure, vibrations develop which then lead to unwanted interior noise through acoustic/structure interactions. Control of this unwanted interior noise is accomplished through sensing and actuating via piezoceramic patches which are bonded to the structure. Before model-based control schemes can be implemented, however, the physical parameters of the structure (which now includes the patches) must be estimated from data which is collected both on the structure and from the acoustic response in the enclosed cavity. Although similarities exist between the problem of estimating physical parameters for the isolated structure and that involving the structural acoustic system, the hyperbolic contributions due to the acoustic component sufficiently change the problem dynamics so as to warrant in-depth study of techniques for the latter coupled system. Finally, we note that although the initial impetus for developing distributed parameter estimation techniques for structural acoustic systems was motivated by model-based noise control considerations, the same techniques can be used when performing vibration analysis or using NDE methods to determine structural flaws in these coupled systems.

The structural acoustic problem used here to motivate and illustrate the development of an appropriate parameter estimation methodology consists of a 2-D enclosed cavity which is separated from the perturbing exterior disturbance by a thin beam. This model represents a 2-D slice from a 3-D model for several experimental apparata being used in the Acoustics Division, NASA Langley Research Center, to test modeling, parameter estimation and control strategies. We add, however, that the methodology being presented is equally valid for estimating parameters in many 3-D models representing various experimental setups currently in use (see the models in [9, 10]). This 2-D model was chosen simply because it simplifies the discussion and more clearly illustrates the process involved in developing the parameter identification techniques.

Moreover, the modeling, mathematical, and computational considerations presented here are valid whether the external source or disturbance of the elastic structure (denoted by f in the model below) is acoustic, mechanical or electromagnetic excitation of the structure. The principle ideas in this paper are also pertinent whether we assume that the piezoceramics are bonded to the structure or are embedded within the structure. For the sake of definiteness, we assume that the piezoceramic patches are bonded to the structure (the structural models are somewhat different if the patches are embedded).

The model being used to illustrate the methodology is weakly nonlinear due to the manner in which the structural vibrations couple with the interior acoustic fields. While linearization provides a very good approximation to the system dynamics (see [1]), we retain the nonlinearity here so as to illustrate some of the general analytic assumptions which are made when extending well-posedness and parameter convergence results for the corresponding linear problem to a weakly nonlinear problem of this type. This also facilitates the demonstration of numerical techniques which can be used when simulating, testing and implementing the parameter estimation scheme in the nonlinear problem. In discussing parameter estimation methods for structural acoustics problems of this type, our emphasis is on the formulation of the problem in a manner which is conducive to approximation and implementation both in the linear and nonlinear forms as well as under a variety of interior cavity damping assumptions.

In the second section of this presentation, a model for the 2-D system being used to illustrate the parameter estimation method is presented. Details regarding the modeling of the acoustic and structural components as well as coupling conditions are given, and care is taken to motivate the assumptions which lead to various damping conditions in the system model. In formulating the strong form of the system model, details are also given regarding the interactions between the piezoceramic patches and the underlying structure (beam) as well as the weakly nonlinear interactions between the beam and the interior acoustic field. To provide a formulation which is conducive to approximation in the context of unbounded input operators as well as facilitates the discussion of well-posedness results, the weak form of the system equations is then developed and posed in terms of sesquilinear forms and the bounded operators which they define. Finally, we show that the solution trajectories can be expressed in terms of a semigroup on an appropriate space and within this framework, the assumptions underlying the well-posedness results for the linear and nonlinear problems are discussed.

A discretization method suitable for simulations and the implementation of the parameter estimation method is outlined in Section 3. This discussion is kept relatively brief since details regarding the corresponding finite dimensional system for the linearized problem can be found in [1]. However, the section does provide additional details concerning the discretization of the nonlinear component of the operator and a brief algorithm for carrying out this discretizetion is included.

A parameter estimation scheme suitable for data consisting of displacement, velocity or acceleration measurements on the beam, voltage measurements from the patches, or pressure measurement inside the cavity is presented in Section 4. Assumptions on the form of the unknown parameters are discussed and conditions leading to convergence and continuous dependence on data results for the linear and nonlinear problems are outlined.

In Section 5, numerical examples demonstrating the parameter estimation techniques with a variety of data types and methods for exciting the system are presented. Specifically, examples are given in which the force to the system is provided by a numerically simulated acoustic source, simulated voltage inputs to the patches, and a simulated hammer impact to the beam. The simulated data under comparison in the examples consists of acceleration values of the beam, voltage (accumulated strain) values from the patches, and voltage values in conjunction with interior acoustic pressure values. The conclusions from this study and physical considerations concerning the implementation of the method are summarized in the final section of the paper.

2 System Model

The model of interest consists of an exterior disturbance which is separated from an interior cavity $\Omega(t)$ by a common elastic boundary $\Gamma_0(t)$ that is modeled by an Euler-Bernoulli beam as depicted in Figure 1. The beam is assumed to have length a, width b and thickness h. The Young's modulus, mass density (in mass per unit volume) and damping coefficient for the homogeneous beam are denoted by E_b, ρ_b and c_{Db}, respectively. Due to the nature of the exterior forces and the manner in which the patches are excited, we will be considering only transverse vibrations $w(t,x)$.

Bonded to the beam are piezoceramic patches which are mounted in pairs as depicted in Figure 1. In this discussion, it is assumed that the patches have thickness T, width b, Young's modulus E_{pe}, density ρ_{pe}, and damping coefficient $c_{D_{pe}}$. Moreover, it is assumed that the bonding layers for each patch have equal thicknesses, Young's moduli, densities and damping coefficients, and these parameters are denoted by $T_{b\ell}$, $E_{b\ell}$, $\rho_{b\ell}$ and $c_{Db\ell}$, respectively. We emphasize that these assumptions are made solely for clarity of presentation, and similar results can be obtained in an analogous manner for the more general case in which the patches and bonding layers have differing thicknesses and material properties (see, for example, [12]).

Finally, we assume that inside the cavity, there is a region $\tilde{\Omega} = \bigcup_{i=1}^{N_R} \tilde{\Omega}_i$, possibly all of Ω, with $\tilde{\Omega} \cap \partial\Omega(t) = \not{\emptyset}$, which provides a first approximation to the interior material (eg., passengers, seats, storage compartments in the case of an aircraft interior; elastic or medium

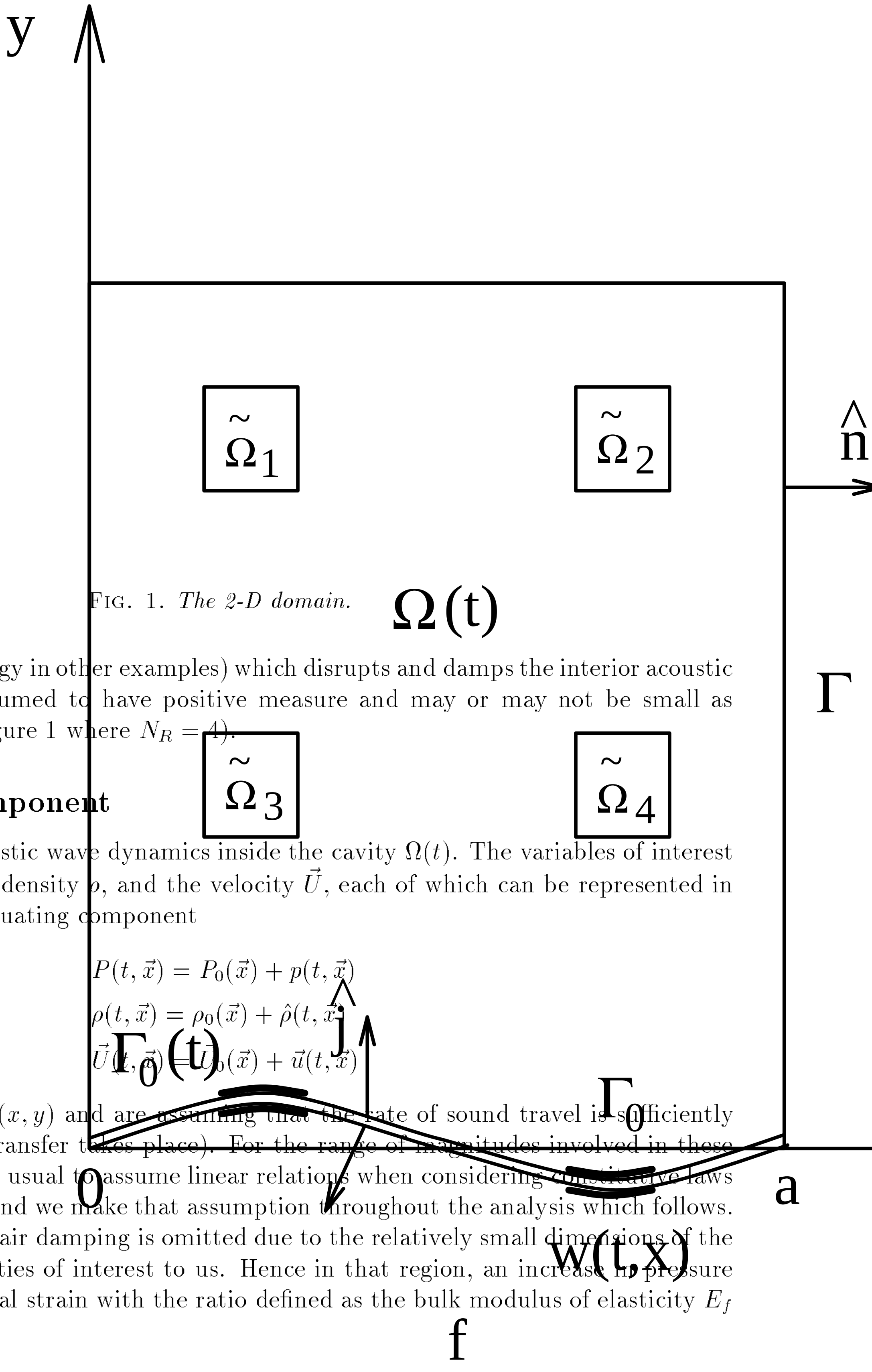

Fig. 1. *The 2-D domain.*

material that absorbs energy in other examples) which disrupts and damps the interior acoustic fields. This region is assumed to have positive measure and may or may not be small as compared to $\Omega(t)$ (see Figure 1 where $N_R = 4$).

2.1 Acoustic Component

We consider first the acoustic wave dynamics inside the cavity $\Omega(t)$. The variables of interest to us are the pressure P, density ρ, and the velocity $\vec{U}$, each of which can be represented in terms of a mean and fluctuating component

$$P(t,\vec{x}) = P_0(\vec{x}) + p(t,\vec{x})$$
$$\rho(t,\vec{x}) = \rho_0(\vec{x}) + \hat{\rho}(t,\vec{x})$$
$$\vec{U}(t,\vec{x}) = \vec{U}_0(\vec{x}) + \vec{u}(t,\vec{x})$$

(here we have taken $\vec{x} = (x,y)$ and are assuming that the rate of sound travel is sufficiently rapid so that little heat transfer takes place). For the range of magnitudes involved in these problems ($<$ 140 dB), it is usual to assume linear relations when considering constitutive laws and force balancing [20], and we make that assumption throughout the analysis which follows.

In the region $\Omega(t) \setminus \tilde{\Omega}$, air damping is omitted due to the relatively small dimensions of the type of experimental cavities of interest to us. Hence in that region, an increase in pressure brings about a proportional strain with the ratio defined as the bulk modulus of elasticity E_f

where

$$E_f = \frac{-p}{\nabla \cdot \vec{s}} \quad \text{or} \quad p = -E_f \nabla \cdot \vec{s} \tag{2.1}$$

($\vec{s}(t, \vec{x})$ denotes the displacement of the center of gravity of an infinitesimal element of the medium and satisfies $\vec{s}_t = \vec{u}$). On the other hand, the material lumped in $\tilde{\Omega}$ will provide some medium damping and here we assume that a change in pressure yields

$$p = -\tilde{E}\nabla \cdot \vec{s} - \tilde{d}\nabla \cdot \vec{s}_t \tag{2.2}$$

where $\tilde{E}$ and $\tilde{d}$ denote the bulk modulus of elasticity and damping coefficient of the medium in $\tilde{\Omega}$. We point out that this use of a generalized Hooke's law in which stress is proportional to a linear combination of strain and strain rate is done under the assumption that relatively low acoustic frequencies are excited ($<$ 1000 Hz), and is similar to the constitutive law leading to Kelvin-Voigt damping of vibrations in elastic materials. We also emphasize that this damping model should be considered as a first approximation to the actual acoustic damping mechanism in the medium $\tilde{\Omega}$, and depending on the specific materials involved, the manner of acoustic excitation, and the geometry of the physical system, more comprehensive models may be required to accurately describe the medium damping.

Force balancing in the acoustic cavity, we obtain the relation (the Euler equation)

$$\rho_0 \frac{\partial^2 \vec{s}}{\partial t^2} = -\nabla p \tag{2.3}$$

where

$$\rho_0 = \begin{cases} \rho_f & , \quad \vec{x} \in \Omega(t)/\tilde{\Omega} \\ \tilde{\rho} & , \quad \vec{x} \in \tilde{\Omega} \end{cases}$$

denotes the equilibrium density of the medium ((2.3) is equivalent to the linearized momentum equation in fluid dynamics). By taking two time derivatives of (2.1) and (2.2), the divergence of (2.3), and eliminating cross terms, one arrives at

$$\begin{aligned} \frac{\partial^2 p}{\partial t^2} &= \frac{E_f}{\rho_f}\Delta p & , \quad \vec{x} \in \Omega(t)/\tilde{\Omega} \\ \frac{\partial^2 p}{\partial t^2} &= \frac{\tilde{E}}{\tilde{\rho}}\Delta p + \frac{\tilde{d}}{\tilde{\rho}}\Delta p_t & , \quad \vec{x} \in \tilde{\Omega}\ . \end{aligned} \tag{2.4}$$

Taking the curl of the momentum equation (2.3) and noting that $\vec{u} = \vec{s}_t$ we obtain $\frac{\partial}{\partial t}(\nabla \times \rho_0 \vec{u}) = 0$. Hence the vorticity $\vec{\omega} = \nabla \times \rho_0 \vec{u}$ is constant in time in $\Omega(t)$. Under the assumption that the initial vorticity $\vec{\omega}(0)$ is zero, we may conclude that $\nabla \times \rho_0 \vec{u} = 0$ for all time or that the flow is irrotational in $\Omega(t)$. Thus in $\Omega(t)$, there exists a scalar velocity potential ϕ such that

$$\rho_0 \vec{u} = -\nabla \phi\ . \tag{2.5}$$

The flow is more complex near and in the region $\tilde{\Omega}$ as a result of the viscous effects and medium damping. This can potentially lead to rotational components in the acoustic field which in general necessitates the use of a vector potential. As a first approximation, however, we are assuming that the rotational components near and in $\tilde{\Omega}$ are negligible and a relation of the form (2.5) will be used throughout the acoustic cavity $\Omega(t)$.

Substituting (2.5) into the momentum equation (2.3) we find

$$\nabla \left\{ \frac{\partial \phi}{\partial t} - p \right\} = 0,$$

which implies that $p = \dfrac{\partial \phi}{\partial t}$ since no acoustic sources or sinks are present in $\Omega(t)$. Use of this pressure expression (actually $p_t = \phi_{tt}$) after differentiation in time once in equations (2.1), (2.2) then yields

$$\begin{aligned} \frac{\partial^2 \phi}{\partial t^2} &= \frac{E_f}{\rho_f} \Delta \phi & , \quad & \vec{x} \in \Omega(t)/\tilde{\Omega} \\ \frac{\partial^2 \phi}{\partial t^2} &= \frac{\tilde{E}}{\tilde{\rho}} \Delta \phi + \frac{\tilde{d}}{\tilde{\rho}} \Delta \phi_t & , \quad & \vec{x} \in \tilde{\Omega} \; . \end{aligned}$$

Finally, hardwall boundary conditions are assumed since one of the experimental configurations (a cylinder with end plates) that we have modeled has concrete walls. With $\hat{n}$ denoting the outward unit normal to the cavity and $c^2(\vec{x})$ and $d(\vec{x})$ denoting the speed of sound and damping coefficients given by

$$c^2(\vec{x}) = \begin{cases} E_f/\rho_f & , \quad \vec{x} \in \Omega(t)/\tilde{\Omega} \\ \tilde{E}/\tilde{\rho} & , \quad \vec{x} \in \tilde{\Omega} \end{cases} \quad , \quad d(\vec{x}) = \begin{cases} 0 & , \quad \vec{x} \in \Omega(t)/\tilde{\Omega} \\ \tilde{d}/\tilde{\rho} & , \quad \vec{x} \in \tilde{\Omega} \; , \end{cases}$$

the acoustic response can be modeled as

$$\begin{aligned} \frac{\partial^2 \phi}{\partial t^2} &= c^2 \Delta \phi + d \Delta \phi_t & , \quad & (x,y) \in \Omega(t) \; , t > 0 \; , \\ \nabla \phi \cdot \hat{n} &= 0 & , \quad & (x,y) \in \Gamma \; , t > 0 \; . \end{aligned} \tag{2.6}$$

We emphasize that this model was derived under the assumption that the only acoustic damping in the cavity occurs in the region $\tilde{\Omega}$ and hence $d(\vec{x}) = 0$ in the rest of the chamber and boundary, i.e. for $\vec{x} \in \Omega(t)/\tilde{\Omega}$ and $\partial\Omega(t) = \Gamma \cup \Gamma_0(t)$. Moreover, we have assumed that the flow is irrotational in the region $\Omega(t)$.

2.2 Beam Component

Through force and moment balancing, the equation of motion for the transverse displacements w of the beam are found to be

$$\begin{aligned} \rho w_{tt} + \frac{\partial^2 \mathcal{M}}{\partial x^2}(t,x) &= -\phi_t(t,x,w(t,x)) + f(t,x) \qquad 0 < x < a \; , \; t > 0 \; , \\ w(t,0) = \frac{\partial w}{\partial x}(t,0) = w(t,a) &= \frac{\partial w}{\partial x}(t,a) = 0 \qquad t > 0 \;\; , \end{aligned}$$

where $\mathcal{M}$ is the total beam moment, f is the force due to the exterior disturbance field and $\phi_t(t,x,w(t,x))$ is the backpressure due to the ensuing acoustic waves inside the cavity (this latter term is in general nonlinear since its effect occurs on the surface of the vibrating beam). For pairs of patches having edges x_1 and x_2, the density of the structure is

$$\rho(x) = \rho_b h b + 2b \left(\rho_{b\ell} T_{b\ell} + \rho_{pe} T \right) \chi_{pe}(x) \tag{2.7}$$

where the characteristic function

$$\chi_{pe}(x) = \begin{cases} 1 & , \quad x_1 \le x \le x_2 \\ 0 & , \quad \text{otherwise} \end{cases}$$

localizes the patch effects between the endpoints x_1 and x_2 (see [11, 12] for details).

The general beam moment

$$\mathcal{M}(t,x) = M(t,x) - M_{pe}(t,x)$$

consists of an internal component M, depending on material and geometric properties of the beam and patches, and an external component M_{pe} (the control term) which results from the activation of the patches through an applied voltage (see Figure 2(a)).

For a beam undergoing pure bending motion with out-of-phase excitation of the patches, the internal and external moments are given by

$$\begin{aligned} M(t,x) &= EI(x)\frac{\partial^2 w}{\partial x^2} + c_D I(x)\frac{\partial^3 w}{\partial x^2 \partial t} \\ M_{pe}(t,x) &= \mathcal{K}^B V \chi_{pe}(x) \end{aligned}$$

where V is the voltage into the patches. As shown in [11], the stiffness, damping and control constants for the combined structure are

$$\begin{aligned} EI(x) &= E_b\frac{h^3 b}{12} + \frac{2b}{3}\left[E_{b\ell}a_{3b\ell} + E_{pe}a_{3pe}\right]\chi_{pe}(x) \\ c_D I(x) &= c_{D_b}\frac{h^3 b}{12} + \frac{2b}{3}\left[c_{D_{b\ell}}a_{3b\ell} + c_{D_{pe}}a_{3pe}\right]\chi_{pe}(x) \\ \mathcal{K}^B &= E_{pe} b d_{31}(h + 2T_{b\ell} + T)\ . \end{aligned} \tag{2.8}$$

The constants $a_{3b\ell}$ and a_{3pe} given by $a_{3b\ell} = (h/2 + T_{b\ell})^3 - (h/2)^3$ and $a_{3pe} = (h/2 + T_{b\ell} + T)^3 - (h/2 + T_{b\ell})^3$ result from the integration of stresses through the bonding layer and patch, and d_{31} is a piezoceramic constant which relates the amount of strain produced in the patch to the level of voltage being applied.

At this point it is worth commenting further on the damping term $c_{D_{pe}}$ which is taken to be a combination of the Kelvin-Voigt damping coefficient for the patch and the damping which results from the production of current when the structure vibrates. This latter contribution to the damping results from the piezoelectric effect of the patches which dictates that a voltage is produced when the patch is subjected to in-plane strains. Under the assumption that the Kelvin-Voigt (material) and electrical damping have approximately the same types of effect in the patch, we have combined the two into the coefficient $c_{D_{pe}}$ which must be considered to be unknown and like the other parameters, must ultimately be estimated using data fitting techniques with experimental data when considering actual applications. We also point out that the expression (2.8) can easily be generalized to include the possibility of differing material properties in the two patches or bonding layers (again, see [11, 12]).

The fact that the patches generate a voltage when strained implies that they can be used as sensors as well as actuators. Specifically, the voltage produced by the patches when the beam bends is

$$V_s(t) = \mathcal{K}^S \int_{x_1}^{x_2} \frac{\partial^2 w}{\partial x^2}(t,x)dx = \mathcal{K}^S \left[\frac{\partial w}{\partial x}(t,x_2) - \frac{\partial w}{\partial x}(t,x_1) \right] \tag{2.9}$$

where the sensor constant $\mathcal{K}^S$ depends upon piezoelectric material properties as well as the geometry and size of the patch (see [18]). Hence the voltage provides a measure of accumulated strain in the beam (see Figure 2(b)) thus enabling the patch to serve as a sensor in a variety of applications involving the measurement of beam vibrations.

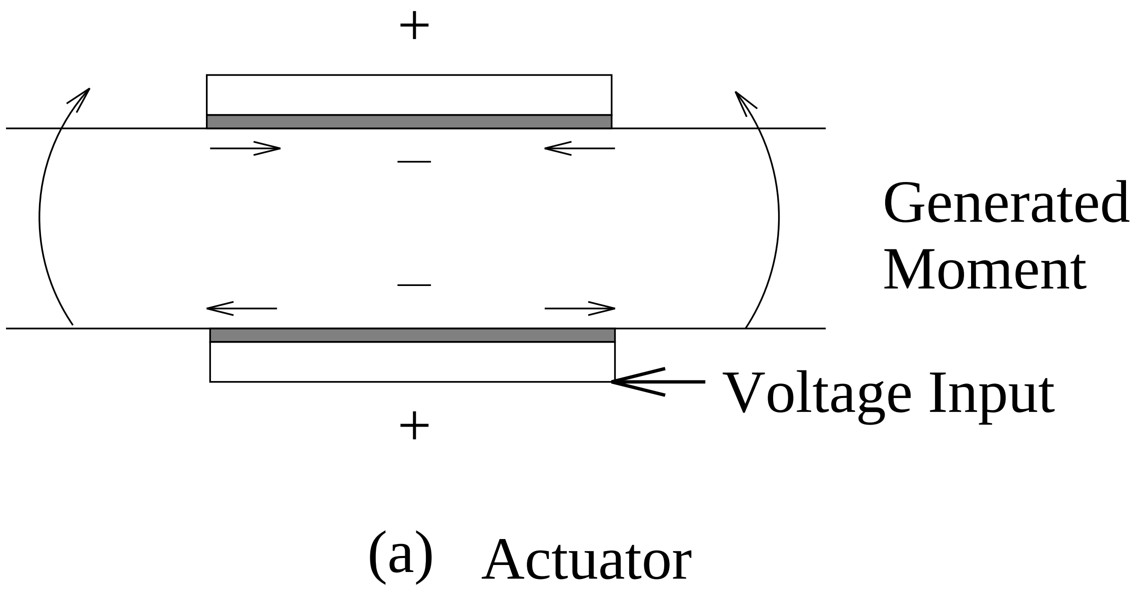

FIG. 2. *Acoustic cavity with piezoceramic patches; (a) patch generation of pure bending moments, (b) patch sensing of accumulated strain, and (c) fixed domain Ω and boundary $\Gamma \bigcup \Gamma_0$.*

2.3 Coupling Conditions

In the model discussed thus far, the structural and internal acoustic responses are coupled through the backpressure $\phi_t(t,x,w(t,x))$ on the surface of the beam. A second coupling equation is the continuity of velocity (or momentum) condition

$$w_t(t,x) = -\frac{1}{\rho_0}\nabla\phi(t,x,w(t,x)) \cdot \hat{\jmath} \; , \quad 0 < x < a \; , t > 0$$

which results from the assumption that the beam is impenetrable to air (or whatever the fluid in the interior cavity). We point out that the velocity condition provides a form of damping to the beam which is similar to that obtained with the incorporation of viscous (air) damping effects (modeled by a term of the form γw_t in the beam equation). As noted in the examples, the internal Kelvin-Voigt damping in concert with the coupling effects due to the continuity of velocity and backpressure causes a beam response which differs somewhat from that observed with an uncoupled, undamped beam having the same dimensions.

The model we have developed has nonlinearities in the (i) variable domain $\Omega(t)$, (ii) back pressure term $-\phi_t(t,x,w(t,x))$, and (iii) velocity term $\frac{1}{\rho_0}\nabla\phi(t,x,w(t,x)) \cdot \hat{\jmath}$.

Accumulated Strain
Generated Voltage
(b) Sensor

2.4 Strong Form of the System Equations

For the coupled system in which s pairs of patches are bonded to the beam and excited out-of-phase, the acoustic, structural and coupling components just discussed can be combined to yield the nonlinear model

$$
\begin{aligned}
&\phi_{tt} = c^2\Delta\phi + d\Delta\phi_t \qquad (x,y)\in\Omega(t)\ , t>0\ ,\\
&\nabla\phi\cdot\hat{n} = 0 \qquad (x,y)\in\Gamma\ , t>0\ ,\\
&-\frac{1}{\rho_0}\nabla\phi(t,x,w(t,x))\cdot\hat{\jmath} = w_t(t,x) \qquad 0<x<a\ , t>0\ ,\\
&\rho w_{tt} + \frac{\partial^2}{\partial x^2}\left(EI\frac{\partial^2 w}{\partial x^2} + c_D I\frac{\partial^3 w}{\partial x^2\partial t}\right)\\
&\qquad = -\phi_t(t,x,w(t,x)) + f(t,x) + \frac{\partial^2}{\partial x^2}\sum_{i=1}^{s}\mathcal{K}_i^B u_i(t)\chi_{pe_i}(x) \qquad \begin{array}{l} 0<x<a\ ,\\ t>0\ ,\end{array}\\
&w(t,0) = \frac{\partial w}{\partial x}(t,0) = w(t,a) = \frac{\partial w}{\partial x}(t,a) = 0 \qquad t>0\ \ ,\\
&\phi(0,x,y) = \phi_0(x,y) \quad , \quad w(0,x) = w_0(x)\\
&\phi_t(0,x,y) = \phi_1(x,y) \quad , \quad w_t(0,x) = w_1(x)\ \ .
\end{aligned}
\tag{2.10}
$$

Here $u_i(t)$ is the voltage being applied to the i^{th} patch and χ_{pe_i} denotes the characteristic function over the i^{th} patch.

We point out that the piezoceramic material parameters $\mathcal{K}_i^S$ (see (2.9)) and $\mathcal{K}_i^B$, $i = 1,\cdots,s$ as well as the beam parameters ρ, EI and $c_D I$ are considered to be unknown and are estimated using inverse problem techniques as discussed in later sections. While the expressions given in (2.7) and (2.8) can be used as starting values in the parameter estimation routines, experimental evidence (see [15, 16]) has indicated that the final parameter values can vary quite significantly from the analytic values due to the contributions from the bonding layer, variation in the measurement of physical constants, and nonuniformities in the various materials. This combined with the lack of analytic expressions for the damping constant necessitates the estimation of these parameters before model-based control strategies can be implemented.

We also emphasize that the parameters $\mathcal{K}_i^B, \rho, EI$ and $c_D I$ are piecewise constant in nature due to the presence and differing material properties of the bonding layer and patches (see (2.8) as well as the results in [15]). This leads to difficulties with the strong form of the system equations since it necessitates the second derivatives of the Heaviside function (equivalently, derivatives of the Dirac delta) thus yielding an unbounded control input operator. The differentiation of the discontinuous material parameters also leads to difficulties when approximating the dynamics of the coupled system. To avoid these problems, it is advantageous to formulate the problem in weak or variational form (the use of the variational form also permits the use of basis functions having less smoothness than required for those used when approximating the solution to the strong form of the equations).

Finally, we note that in the case of no acoustic cavity damping ($d \equiv 0$ and $\rho_0 = \rho_f$), the model (2.10) is completely equivalent to the nonlinear models whose linearizations are the basis of the investigations in [1, 8, 10, 11] if one makes the approximation $-\nabla\phi \cdot \hat{\jmath} \approx \nabla\phi \cdot \hat{n}$ and replaces the coupling terms $\rho_f \phi_t$ and $\vec{v} = -\nabla\phi$ in those models by ϕ_t and $\vec{v} = -\frac{1}{\rho_f}\nabla\phi$, respectively. That is, the potential used in those references differs from the one used here by a multiplicative factor $\frac{1}{\rho_f}$.

2.5 Weak Form of the System Equations

An appropriate choice for the state of the second-order problem (2.10) is the pair (ϕ, w) consisting of the acoustic potential and beam displacement. It follows immediately that with this choice, the state for the problem in first-order form is $\mathcal{Z} = (\phi, w, \dot{\phi}, \dot{w})$ which contains the pressure (since $p = \dot{\phi}$) as well as the beam displacement and velocity.

To facilitate the writing of (2.10) in weak form we make several assumptions. First we assume that $\nabla\phi(t, x, w(t, x)) \cdot (\hat{\jmath} + \hat{n})$ is small (this is reasonable if either $\nabla\phi$ is small near $\Gamma_0(t)$ or if the beam has small slope so that $-\hat{\jmath} \approx \hat{n}$). Note that with this assumption, the velocity term $-\frac{1}{\rho_0}\nabla\phi(t, x, w(t, x)) \cdot \hat{\jmath}$ in (2.10) can be approximated by the normal term $\frac{1}{\rho_0}\nabla\phi(t, x, w(t, x)) \cdot \hat{n}$ which arises when developing the weak form of the equation. In addition to making this approximation, we multiply the cavity and beam equations in (2.10) by sufficiently smooth test functions ξ and η, respectively, and integrate by parts (Green's theorem) in the usual manner (see[1]). Assuming that η satisfies the boundary conditions $\eta(x) = \eta'(x)$ at $x = 0$ and $x = a$, we then obtain

$$\begin{aligned}
&\int_{\Omega(t)} \left\{ \frac{1}{\rho_0 c^2}(\dot{\phi})_t \xi + \frac{1}{\rho_0}\nabla\phi \cdot \nabla\xi + \frac{d}{\rho_0 c^2}\nabla\dot{\phi} \cdot \nabla\xi \right\} dw \\
&\quad - \int_{\Gamma_0(t)} \dot{w}\xi \, d\gamma + \int_{\Gamma_0} \left\{ \rho \dot{w}_t \eta + EID^2 w D^2 \eta c_D I D^2 \dot{w} D^2 \eta + \dot{\phi}(w)\eta \right\} d\gamma \qquad (2.11) \\
&\quad = \int_{\Gamma_0} \sum_{i=1}^{s} \mathcal{K}_i^B u_i(t) \chi_{pe_i} D^2 \eta d\gamma + \int_{\Gamma_0} f\eta d\gamma.
\end{aligned}$$

In the integrals above we make the further approximations that $\int_{\Omega(t)} = \int_\Omega$ where Ω is the fixed domain $\Omega \equiv [0, a] \times [0, \ell]$, and $\int_{\Gamma_0(t)} = \int_{\Gamma_0}$ where Γ_0 is the boundary $0 < x < a, \ y = 0$ as depicted in Figure 2(c). We then obtain the nonlinear first order variational form

$$\begin{aligned}
&\int_\Omega \frac{1}{\rho_0 c^2} \left(\dot{\phi}\right)_t \xi d\omega + \int_{\Gamma_0} \rho \dot{w}_t \eta d\gamma \\
&\quad + \int_\Omega \frac{1}{\rho_0}\nabla\phi \cdot \nabla\xi d\omega + \int_{\Gamma_0} EID^2 w D^2 \eta d\gamma \\
&\quad + \int_\Omega \frac{1}{\rho_0 c^2} d \, \nabla\dot{\phi} \cdot \nabla\xi d\omega + \int_{\Gamma_0} \left\{ c_D I D^2 \dot{w} D^2 \eta + \left[\dot{\phi}(w)\eta - \dot{w}\xi\right] \right\} d\gamma \qquad (2.12) \\
&\quad = \int_{\Gamma_0} \sum_{i=1}^{s} \mathcal{K}_i^B u_i(t) \chi_{pe_i} D^2 \eta d\gamma + \int_{\Gamma_0} f\eta d\gamma
\end{aligned}$$

for all $\Psi = (\xi, \eta) \in V$.

The state space and space of test functions are taken to be the product spaces $\mathcal{H} = V \times H$ and $\mathcal{V} = V \times V$ where the Hilbert spaces H and V are given by $H = \bar{L}^2(\Omega) \times L^2(\Gamma_0)$ and $V = \bar{H}^1(\Omega) \times H_0^2(\Gamma_0)$. Here $\bar{L}^2(\Omega)$ and $\bar{H}^1(\Omega)$ denote the quotient spaces of L^2 and H^1 over the constant functions and $H_0^2(\Gamma_0)$ is given by $H_0^2(\Gamma_0) = \{\psi \in H^2(\Gamma_0) : \psi(x) = \psi'(x) = 0 \text{ at } x = 0, a\}$ (the use of the quotient space results from the fact that the potentials are determined only up to a constant). From energy considerations, the H and V inner products are taken to be

$$\left\langle \begin{pmatrix} \phi \\ w \end{pmatrix}, \begin{pmatrix} \xi \\ \eta \end{pmatrix} \right\rangle_H = \int_\Omega \frac{1}{\rho_0 c^2} \phi \xi d\omega + \int_{\Gamma_0} \rho w \eta d\gamma$$

$$\left\langle \begin{pmatrix} \phi \\ w \end{pmatrix}, \begin{pmatrix} \xi \\ \eta \end{pmatrix} \right\rangle_V = \int_\Omega \frac{1}{\rho_0} \nabla\phi \cdot \nabla\xi d\omega + \int_{\Gamma_0} EID^2 w D^2 \eta d\gamma$$

while the product space inner products are given by

$$\left\langle \begin{pmatrix} \Phi \\ \Psi \end{pmatrix}, \begin{pmatrix} \Upsilon \\ \Lambda \end{pmatrix} \right\rangle_{\mathcal{H}} = \langle \Phi, \Upsilon \rangle_V + \langle \Psi, \Lambda \rangle_H$$

$$\left\langle \begin{pmatrix} \Phi \\ \Psi \end{pmatrix}, \begin{pmatrix} \Upsilon \\ \Lambda \end{pmatrix} \right\rangle_{\mathcal{V}} = \langle \Phi, \Upsilon \rangle_V + \langle \Psi, \Lambda \rangle_V \ .$$

We point out that in the variational form the derivatives have been transferred from the plate and patch moments onto the test functions. This eliminates the problem of having to approximate the derivatives of the characteristic function and the Dirac delta as is the case with the strong form of the equations. Moreover, we note that the continuity of velocity condition $-\frac{1}{\rho_0}\nabla\phi \cdot \hat{\jmath} = w_t$ of the strong form becomes a natural boundary condition in the weak or variational form (2.11). Hence it is not directly imposed on any numerical approximate solutions. The coupling condition will therefore be satisfied only approximately in computational solutions as well as in the conceptual formulation given in making the approximation to pass from the strong form (2.10) to the variational form (2.12).

The system (2.12) can be formally approximated by replacing the state variables by their finite dimensional approximations and constructing the resulting matrix system, and it is in this form that we will consider approximation strategies in Section 4. In order to discuss the well-posedness of the problem, however, it is advantageous to pose the problem in an abstract Cauchy format as discussed in the next subsection.

2.6 Abstract First Order Formulation

Following the theoretical work in [2, 3], it is advantageous to formulate the problem in terms of sesquilinear forms and the bounded operators which they define (see also [1, 10] for further examples detailing the abstract formulation of structural acoustic systems in this manner). We begin by pointing out that the Hilbert spaces H and V form a Gelfand triple $V \hookrightarrow H \simeq H^* \hookrightarrow V^*$ with pivot space H (further details concerning the basic definitions and fundamental functional analysis theory here can be found in [22]). For $\Phi = (\phi, w)$ and $\Psi = (\xi, \eta)$ in V, we then define the sesquilinear forms $\sigma_i : V \times V \to \mathcal{C},\ i = 1,2$ by

$$\begin{aligned}
\sigma_1(\Phi,\Psi) &= \int_\Omega \frac{1}{\rho_0}\nabla\phi\cdot\nabla\xi d\omega + \int_{\Gamma_0} EID^2wD^2\eta d\gamma \ , \\
\sigma_2(\Phi,\Psi) &= \int_\Omega \frac{1}{\rho_0 c^2} d\ \nabla\phi\cdot\nabla\xi d\omega + \int_{\Gamma_0} \left\{c_D ID^2wD^2\eta + [\phi\eta - w\xi]\right\} d\gamma \ .
\end{aligned} \tag{2.13}$$

With these definitions, it is straightforward to show that σ_1 and σ_2 satisfy various continuity, symmetry and coercivity conditions. Namely, σ_1 satisfies

$$\begin{aligned}
&|\sigma_1(\Phi,\Psi)| \le c_1|\Phi|_V|\Psi|_V \ \ , \text{ for some } \ c_1 \in \mathbb{R} && \text{(bounded)} \\
&\text{Re } \sigma_1(\Phi,\Phi) \ge c_2|\Phi|_V^2 \ \ , \text{ for some } \ c_2 > 0 && (V\text{-elliptic}) \\
&\sigma_1(\Phi,\Psi) = \overline{\sigma_1(\Psi,\Phi)} && \text{(symmetric)}
\end{aligned} \tag{2.14}$$

for all $\Phi,\Psi \in V$ (the boundedness results from Schwarz's inequality for inner products in conjunction with equivalence results for various Sobolev norms, while the V-ellipticity and symmetry of σ_1 follow directly from the fact that $\sigma_1(\Phi,\Psi) = \langle\Phi,\Psi\rangle_V$).

The properties of σ_2 depend upon the form of damping in the cavity Ω. If damping is included in a region $\tilde\Omega \subseteq \Omega$ as discussed in Section 2.1 with $meas(\Omega\setminus\tilde\Omega) = 0$, then σ_2 satisfies

$$\begin{aligned}
&|\sigma_2(\Phi,\Psi)| \le c_3|\Phi|_V|\Psi|_V \ \ , \text{ for some } \ c_3 \in \mathbb{R} && \text{(bounded)} \\
&\text{Re } \sigma_2(\Phi,\Phi) \ge c_4|\Phi|_V^2 \ \ , \text{ for some } \ c_4 > 0 && (V\text{-elliptic}) \ .
\end{aligned} \tag{2.15}$$

The V-ellipticity follows from the fact that

$$\begin{aligned}
\text{Re } \sigma_2(\Phi,\Phi) &= \int_{\tilde\Omega} \frac{d}{\rho_0 c^2}\, |\nabla\phi|^2 d\omega + \int_{\Gamma_0} c_D I\left(D^2w\right)^2 d\gamma \\
&\ge k_1\int_{\tilde\Omega} |\nabla\phi|^2 d\omega + k_2\int_{\Gamma_0} EI\left(D^2w\right)^2 d\gamma \\
&\ge c_4|\Phi|_V^2
\end{aligned}$$

with the final inequality resulting from the observation that $\int_{\tilde\Omega} |\nabla\phi|^2 d\omega = \int_\Omega |\nabla\phi|^2 d\omega$ for all $\Phi \in V$. On the other hand, if the cavity is taken with medium damping in $\tilde\Omega$ with $meas(\Omega\setminus\tilde\Omega) > 0$ (the case of "weak cavity damping"), then one can only establish the weaker H-semiellipticity condition

$$\text{Re } \sigma_2(\Phi,\Phi) \ge c_4|\Phi|_H^2 \ \ , \ c_4 \ge 0 \quad (H - \text{semielliptic})$$

for σ_2 (in this case $c_4 = 0$ since $\sigma_2(\Phi,\Phi)$ contains no full acoustic component when damping is weak in the cavity). As discussed in the next section, the inclusion of medium damping within the region $\tilde\Omega$ where $meas(\Omega\setminus\tilde\Omega) = 0$ and the resulting V-elliptic behavior of σ_2 yields stronger semigroup results than those obtained when acoustic damping is weaker or omitted.

To account for the patch contributions when a voltage is applied, we let U denote the Hilbert space containing the voltage inputs and we define the operator $B \in \mathcal{L}(U, V^*)$ by

$$\langle Bu, \Psi \rangle_{V^*,V} = \int_{\Gamma_0} \sum_{i=1}^{s} \mathcal{K}_i^B u_i \chi_{pe_i} D^2 \eta d\gamma$$

for $\Psi \in V$, where $\langle \cdot, \cdot \rangle_{V^*,V}$ is the usual duality pairing. Finally, the external forcing and nonlinear perturbation terms are given by $F = (0, f/\rho_b)$ and $G(z, z_t) = (0, -\tilde{\phi}_t(w))$ where $\tilde{\phi}_t(w) = \tilde{\phi}_t(t, x, w(t, x)) \equiv \phi_t(t, x, w(t, x)) - \phi_t(t, x, 0)$ denotes the nonlinear perturbation to the linear coupling term.

With these definitions, we can write the system (2.12) in the abstract weak or variational form

$$\langle z_{tt}(t), \Psi \rangle_{V^*,V} + \sigma_2(z_t(t), \Psi) + \sigma_1(z(t), \Psi) = \langle Bu(t) + F + G(z, z_t), \Psi \rangle_{V^*,V} \tag{2.16}$$

for Ψ in V. We reiterate that the state for the problem in second-order form is given by $z(t) = (\phi(t, \cdot, \cdot), w(t, \cdot))$ in $V \hookrightarrow H$.

To pose the system in first-order form, we form the product space terms $\mathcal{B}u(t) = (0, Bu(t))$, $\mathcal{F}(t) = (0, F(t))$ and $\mathcal{G}(\mathcal{Z}(t)) = (0, G(z(t), z_t(t)))$ in $\mathcal{V}^* = V \times V^*$ and define the operators $A_1, A_2 \in \mathcal{L}(V, V^*)$ by

$$\langle A_i \Phi, \Psi \rangle_{V^*,V} = \sigma_i(\Phi, \Psi)$$

for $i = 1, 2$ (the existence of A_1 and A_2 is guaranteed by the boundedness of σ_1 and σ_2). Then, for the state $\mathcal{Z}(t) = (z(t), z_t(t)) = (\phi, w, \dot{\phi}, \dot{w})$ in $\mathcal{H} = V \times H$, the weak form (2.16) is *formally* equivalent to the system

$$\mathcal{Z}_t(t) = \mathcal{A}\mathcal{Z}(t) + \mathcal{C}(t, \mathcal{Z}(t)) \tag{2.17}$$

in $\mathcal{V}^*$ where

$$\mathcal{C}(t, \mathcal{Z}(t)) = \mathcal{B}u(t) + \mathcal{F}(t) + \mathcal{G}(\mathcal{Z}(t)) \tag{2.18}$$

and

$$\text{dom}\, \mathcal{A} = \{\Theta = (\Upsilon, \Lambda) \in \mathcal{H} : \Lambda \in V, A_1\Upsilon + A_2\Lambda \in H\}$$

$$\mathcal{A} = \begin{bmatrix} 0 & I \\ -A_1 & -A_2 \end{bmatrix}. \tag{2.19}$$

(further details concerning the formulation of the first-order system in the linear case can be found in [1]). The representation (2.17) is formal in the sense that the manner in which differentiation and the resulting solution exists has yet to be specified. This will be discussed next in the context of proving well-posedness results for the system model.

Finally, in discussing well-posedness results and parameter convergence in the sections which follow, it proves useful to compare the nonlinear system with that which results when both coupling terms are linearized. The latter is found by replacing the term $\phi_t(t, x, w)$ by $\phi_t(t, x, 0)$ in the various expressions for the coupled system (equivalently, take $G(z, z_t) = 0$). This yields the second-order variational form

$$\langle z_{tt}(t), \Psi \rangle_{V^*,V} + \sigma_2(z_t(t), \Psi) + \sigma_1(z(t), \Psi) = \langle Bu(t) + F, \Psi \rangle_{V^*,V} \tag{2.20}$$

for $\Psi \in V$ and consequently the first-order system

$$\mathcal{Z}_t(t) = \mathcal{A}\mathcal{Z}(t) + \mathcal{B}u(t) + \mathcal{F}(t) \tag{2.21}$$

in $\mathcal{V}^*$.

2.7 Model Well-Posedness

While the main purpose of the paper is the careful modeling presented above and the demonstration (by examples in Section 5 below) of a feasible numerical approach to estimation of parameters, we give here a brief discussion of possible theoretical considerations. The ideas we discuss are admittedly incomplete but they do make a start on well-posedness of the full nonlinear structural acoustics model.

The first step in determining the well-posedness of the semilinear system model is to argue that $\mathcal{A}$ generates a semigroup on $\mathcal{H}$. As noted earlier, the sesquilinear form σ_1 is V-elliptic, continuous and symmetric while σ_2 is continuous and V-elliptic if strong damping ($meas(\Omega \setminus \tilde{\Omega}) = 0$) is included via the region $\tilde{\Omega}$ or H-semielliptic if damping is weak or omitted in the cavity. In both cases, the Lumer-Philips theorem (with arguments similar to those given in pages 82-84 of [2]) can be used to prove that the operator $\mathcal{A}$ defined in (2.19) generates a C_0-semigroup $\mathcal{T}(t)$ on the state space $\mathcal{H}$. The semigroup satisfies the exponential bound $|\mathcal{T}(t)| \leq e^{\omega t}$ for $t \geq 0$ (where in fact, $\omega = 0$ due to the fact that $\mathcal{A}$ is dissipative as shown in [2]). Moreover, if strong medium damping is included via the region $\tilde{\Omega}$ (which implies that σ_2 is V-elliptic), the semigroup $\mathcal{T}(t)$ is analytic on $\mathcal{H}$.

For the problem thus posed, the state lies in $\mathcal{H}$ which implies that the semigroup $\mathcal{T}(t)$ generated by $\mathcal{A} : \text{dom}\, \mathcal{A} \subset \mathcal{H} \to \mathcal{H}$ is defined on $\mathcal{H}$. The nonlinear forcing term $\mathcal{C}(t, \mathcal{Z}(t)) = \mathcal{B}u(t) + \mathcal{F}(t) + \mathcal{G}(\mathcal{Z}(t))$, however, lies in $\mathcal{V}^*$ rather than $\mathcal{H}$ since the control term $B \in \mathcal{L}(U, V^*)$ defines the product space control term $\mathcal{B}u(t) = (0, Bu(t)) \in \{0\} \times V^* \subset V \times V^* = \mathcal{V}^*$. To remedy this, "extrapolation space" ideas and arguments similar to those presented in [3, 4, 19] are used to extend the semigroup $\mathcal{T}(t)$ on $\mathcal{H}$ to a semigroup $\tilde{\mathcal{T}}(t)$ on a larger space $\mathcal{W}^* \supset \{0\} \times V^*$ so as to be compatible with the forcing term.

As detailed in [10], the space of interest is defined in terms of dom $\mathcal{A}^*$ where

$$\text{dom}\, \mathcal{A}^* = \{\chi = (\Phi, \Psi) \in \mathcal{H} | \Psi \in V, A_1^*\Phi - A_2^*\Psi \in H\}$$

$$\mathcal{A}^*\chi = \begin{pmatrix} -\Psi \\ A_1^*\Phi - A_2^*\Psi \end{pmatrix} .$$

Specifically, the space $\mathcal{W} = [\text{dom}\, \mathcal{A}^*]$ is taken to be dom $\mathcal{A}^*$ with the inner product

$$\langle \Phi, \Psi \rangle_{\mathcal{W}} = \langle (\lambda_0 - \mathcal{A}^*)\Phi, (\lambda_0 - \mathcal{A}^*)\Psi \rangle_{\mathcal{H}}$$

for some arbitrary but fixed λ_0 with $\lambda_0 > \omega$ (recall that the original solution semigroup satisfies the bound $|\mathcal{T}(t)| \leq e^{\omega t}$). As proven in [4], the resulting $\mathcal{W}$ norm is equivalent to the graph norm corresponding to $\mathcal{A}^*$. Moreover, we have that $\{0\} \times V^* \subset \mathcal{W}^* = [\text{dom}\, \mathcal{A}^*]^*$ (see [10] for details).

From the definition of $\mathcal{A}^*$ and the equivalence of the $\mathcal{W}$ norm with the graph norm corresponding to $\mathcal{A}^*$, we can define $\tilde{\mathcal{A}}\Theta \in \mathcal{W}^*$ by

$$\left(\tilde{\mathcal{A}}\Theta\right)(\chi) = \langle \Theta, \mathcal{A}^*\chi \rangle_{\mathcal{H}}$$

for all $\Theta \in \mathcal{H}$, $\chi \in \mathcal{W}$. With this definition and the Riesz representation theorem, it is shown in [10] that $\tilde{\mathcal{A}}$ is an extension of the original operator $\mathcal{A}$ from $\operatorname{dom} \mathcal{A} \subset \mathcal{H}$ to all of $\mathcal{H}$. Finally, as proven in [4], the operator $\tilde{\mathcal{A}}$ is the infinitesimal generator of a C_0-semigroup $\tilde{\mathcal{T}}(t)$ on $\mathcal{W}^*$ which is an extension of $\mathcal{T}(t)$ from $\mathcal{H}$ to $\mathcal{W}^*$ (note that $\tilde{\mathcal{T}}(t)$ is also analytic if strong medium cavity damping is included).

Having extended the operator $\mathcal{A}$ and hence the generated semigroup to a space which is compatible with the forcing function, we are now in a position to discuss criteria on the input terms F and B which guarantee the existence of a unique solution to the system model. In the corresponding linear problem, under reasonable regularity conditions on $t \mapsto u(t)$ and $t \mapsto F(t)$, one can immediately argue the existence of a unique strong solution to the system in terms of the extended semigroup $\tilde{\mathcal{T}}(t)$. For the semilinear problem of interest, however, the nonlinear nonhomogeneous terms must satisfy certain continuity criteria in order to obtain similar results. For example, if we let X denote the reflexive Banach space $\mathcal{W}^*$ and assume that $\mathcal{C} : [0,T] \times X \to X$ defined in (2.18) is continuous in t on $[0,T]$ and uniformly Lipschitz continuous on X, then the integral equation

$$\mathcal{Z}(t) = \tilde{\mathcal{T}}(t)\mathcal{Z}_0 + \int_0^t \tilde{\mathcal{T}}(t-s) \begin{pmatrix} 0 \\ Bu(s) + F(s) + G(\mathcal{Z}(s)) \end{pmatrix} ds \tag{2.22}$$

is well-defined for $Bu + F + G(\mathcal{Z}) \in L^2((0,T), V^*)$. Moreover, for $\mathcal{Z}(0) = \mathcal{Z}_0$, the solution $\mathcal{Z}(t)$ of (2.22) is a unique mild solution to (2.17) (see Theorem 1.2, page 184 of [21]). In addition, if $\mathcal{C} : [0,T] \times X \to X$ is Lipschitz continuous in both variables, then it follows from Theorem 1.6, page 189 of [21] that (2.22) provides the strong solution to (2.17) interpreted in the $\mathcal{W}^*$ sense.

The required continuity of the nonhomogeneous terms Bu and F is demonstrated in [10] and hence the remaining question concerns the Lipschitz continuity of the nonlinear coupling term $G(z, z_t) = (0, -\tilde{\phi}_t(w))$. This is a difficult condition to assure *a priori*. However, if we assume that the input terms F and Bu are sufficiently smooth so as to assure the necessary continuity in $G(z, z_t)$, then the nonlinear system is well-posed. These results are summarized in the following result.

Lemma 1. (Well-Posedness of the Nonlinear System) Consider the nonlinear system represented by (2.16), (2.17) or (2.22) and assume that F and Bu are sufficiently smooth so that $\mathcal{C}(t, \mathcal{Z}(t)) = \mathcal{B}u(t) + \mathcal{F}(t) + \mathcal{G}(\mathcal{Z}(t))$ is Lipschitz continuous in both t and $\mathcal{Z}$. Then (2.22) with $\mathcal{Z}_0 \in \mathcal{H}$ is the unique strong solution to (2.16) both when strong acoustic cavity damping is assumed and when weak or no damping is present in the cavity (in which case, σ_2 is only H-semielliptic).

These results can be further extended when strong acoustic damping is assumed via the region $\tilde{\Omega}$ and hence σ_2 is V-elliptic and $\tilde{\mathcal{T}}(t)$ is analytic. In this case, the mild (and thus strong) solutions to (2.21) are guaranteed to be equivalent to the weak or variational solutions to (2.20) for sufficiently smooth nonhomogeneous terms. Moreover, the following theorem summarizes the corresponding result for the linearized problem.

Theorem 1. (Linearized System: Equivalence of Solutions) Consider the system represented by (2.20) or (2.21) and suppose that the mappings $t \mapsto u(t)$ and $t \mapsto F(t)$ from $[0, T]$ to $\mathbb{R}^1$ and V^*, respectively, are Lipschitz continuous. Furthermore, assume that medium damping of the form (2.2) is present in the region $\tilde{\Omega}$ with $meas(\Omega \setminus \tilde{\Omega}) = 0$. Then for each $\mathcal{Z}_0 \in \mathcal{H} = \mathrm{dom}\, \tilde{\mathcal{A}}$, we have that (2.21) taken with $\mathcal{Z}(0) = \mathcal{Z}_0$ has a unique strong solution given by (2.22) with $\mathcal{G}(\mathcal{Z}) = 0$. Moreover, this strong solution is equal to the weak solution of (2.20).

The proof of the equivalency between strong and weak solutions follows that given in [3] for general second-order systems with unbounded input terms. We point out that numerous numerical results have suggested similar results for the nonlinear problem and the case in which damping is omitted in the cavity even though we have not been able to extend the results equating the strong and weak solutions to cover those cases.

3 State Approximation

The modeling and well-posedness discussion thus far has been for the infinite dimensional nonlinear structural acoustic system. In this section we discuss a Galerkin scheme for discretizing the problem which can be used when simulating the system dynamics, estimating the physical parameters, and calculating control gains (see [1]). This is accomplished by approximating the beam displacement and acoustic potential by spline and spectral expansions, respectively.

3.1 System Approximation

As detailed in [1] where the corresponding linear problem was considered, cubic splines are suitable for discretizing the beam displacement since they satisfy the smoothness requirement as well as being easily implemented when adapting to the fixed-end boundary conditions and patch discretizations. Specifically, the approximate beam displacement is taken to be the linear combination

$$w^N(t,x) = \sum_{i=1}^{n-1} w_i^N(t) B_i^n(x)$$

where B_i^n is the i^{th} cubic spline which has been modified to satisfy the boundary conditions.

The acoustic potential is approximated by the Galerkin expansion

$$\phi^N(t,x,y) = \sum_{j=0}^{m_y} \sum_{\substack{i=0 \\ i+j\neq 0}}^{m_x} \phi_{ij}^N(t) P_i^a(x) P_j^\ell(y)$$

where $P_i^a(x)$ and $P_i^\ell(y)$ denote the standard Legendre polynomials that have been scaled by transformation to the intervals $[0,a]$ and $[0,\ell]$, respectively. The condition $i+j\neq 0$ eliminates the constant function thus guaranteeing that the set of functions is suitable as a basis for the quotient space. We take $\{B_k(x,\theta)\}_{k=1}^m = \{P_i^a(x)P_j^\ell(y)\}_{i,j=1,i+j\neq 0}^{m_x,m_y}$ where $m\equiv (m_x+1)(m_y+1)-1$.

The m and $n-1$ dimensional approximating cavity and beam subspaces are taken to be $H_c^m = \text{span}\,\{B_i^m\}_{i=1}^m$ and $H_b^n = \text{span}\,\{B_i^n\}_{i=1}^{n-1}$, respectively, where B_i^m and B_i^n are the i^{th} cavity and beam bases described above. Defining $N=m+n-1$, the approximating state space is then taken to be $H^N = H_c^m \times H_b^n$ and the product space for the first order system is $\mathcal{H}^N = H^N\times H^N$.

By restricting the infinite dimensional system (2.12) to $\mathcal{H}^N\times\mathcal{H}^N$, one obtains the nonlinear finite dimensional system

$$\begin{bmatrix} M_1^N & 0\\ 0 & M_2^N\end{bmatrix}\begin{bmatrix}\dot\vartheta^N(t)\\ \ddot\vartheta^N(t)\end{bmatrix} = \begin{bmatrix} 0 & M_1^N\\ -A_1^N & -A_2^N\left(w^N(t)\right)\end{bmatrix}\begin{bmatrix}\vartheta^N(t)\\ \dot\vartheta^N(t)\end{bmatrix} + \begin{bmatrix}0\\ \tilde B^N\end{bmatrix}u(t) + \begin{bmatrix}0\\ \tilde F^N(t)\end{bmatrix}$$

$$\begin{bmatrix} M_1^N & 0\\ 0 & M_2^N\end{bmatrix}\begin{bmatrix}\vartheta^N(0)\\ \dot\vartheta^N(0)\end{bmatrix} = \begin{bmatrix} g_1^N\\ g_2^N\end{bmatrix}$$

with

$$\begin{aligned} &M_1^N = \text{diag}[M_{11}^N, M_{12}^N]\ ,\\ &M_2^N = \text{diag}[M_{21}^N, M_{22}^N]\ ,\quad A_2^N\left(w^N(t)\right) = \begin{bmatrix} 0 & A_{31}^N\\ A_{32}^N\left(w^N(t)\right) & A_{22}^N\end{bmatrix}\\ &A_1^N = \text{diag}[A_{11}^N, A_{12}^N]\end{aligned}$$

and

$$\tilde B^N = \left[0, \tilde B_2^N\right]^T \quad , \quad \tilde F^N(t) = \left[0, \tilde F_2^N(t)\right]^2 \ .$$

The vector $\vartheta^N(t) = (\phi_1^N(t), \phi_2^N(t),\cdots,\phi_m^N(t), w_1^N(t), w_2^N(t),\cdots, w_{n-1}^N(t))^T$ contains the $N\times 1 = (m+n-1)\times 1$ approximate state coefficients while $u(t) = (u_1(t),\cdots u_s(t))^T$ contains the s voltage values. The matrices M_{21}^N and A_{11}^N are the mass and stiffness matrices which arise when solving the uncoupled wave equation with Neumann boundary conditions while M_{22}^N, A_{12}^N and A_{22}^N are the mass, stiffness and damping matrices which arise when solving the damped beam equation with fixed boundary conditions. The matrices M_{11}^N and M_{12}^N result from the choice of V inner product (see [1]). The contributions from the coupling terms are contained in the matrix A_{31}^N and operator $A_{32}^N(w^N(t))$ while the control, forcing and initial terms are contained in $\tilde B_2^N$, $\tilde F_2^N(t)$ and $\tilde y_0^N$, respectively. A more detailed description of how the various component matrices are constructed can be found in [1].

The equivalent finite dimensional Cauchy equation is then

$$\begin{aligned} \dot y^N(t) &= \mathcal{A}^N\left(y^N(t)\right) + B^N u(t) + F^N(t)\\ y^N(0) &= \tilde y_0^N\end{aligned} \tag{3.1}$$

with the various operator definitions following from those given above. As with the infinite dimensional problem, it will also be useful to consider the corresponding problem

$$\begin{aligned} \dot{y}^N(t) &= A^N y^N(t) + B^N u(t) + F^N(t) \\ y^N(0) &= \tilde{y}_0^N \end{aligned} \tag{3.2}$$

when considering issues such as parameter convergence. The linear operator A^N is obtained by considering the linearization of $A_{32}^N(w^N(t))$ as discussed in [1].

3.2 Algorithm for Constructing the Nonlinear Component

The determination of state trajectories involves the repeated construction of the nonlinear operator $\mathcal{A}^N(y^N(t))$. Although most of the components of this operator need to be constructed only once, the $(n-1)\times m$ matrix $A_{32}^N(w^N(t))$ must be determined at each step in the solution of the ordinary differential equation (ODE) (3.1) and hence its formation must be made as efficient as possible.

We first point out that for $i,j = 1,\cdots,m_x,m_y$, this $(n-1)\times m$ matrix has the entries

$$\left[A_{32}^N\left(w^N(t)\right)\right]_{p,ij} = \int_0^a B_p^n(x)P_i^a(x)P_j^\ell(\sum_{J=1}^{n-1} w_J^N(t)B_J^n(x))\,dx$$

where the integrals are evaluated via a Gaussian quadrature rule of the form

$$\int_0^a f(x)dx \approx \sum_{k=1}^{n_q} c_k f(x_k)\ .$$

Here n_q is the number of quadrature points and c_k is the quadrature weight. These quadratures and hence the formation of the matrix can be efficiently accomplished in the manner outlined in the following algorithm.

Numerical Algorithm for Creating the Nonlinear Component $A_{32}^N\left(w^N(t)\right)$:

1. Create the matrices A_{32a}^N, A_{32aw}^N and A_{32bj1}^N which have the components

$$\left[A_{32a}^N\right]_{ik} = B_k^n(x_i) \quad , \quad \left[A_{32aw}^N\right]_{ki} = c_k B_k^n(x_i) \quad , \quad \left[A_{32bj1}^N\right]_{ij} = P_j^a(x_i)$$

   (hence $\dim A_{32a}^N = n_q\times(n-1)$, $\dim A_{32aw}^N = (n-1)\times n_q$ and $\dim A_{32bj1}^N = n_q\times(m_x+1)$). These matrices need to be formed *only once* and can be created before solving the ODE system.

2. With the notation $\circ$ denoting Hadamard or componentwise multiplication, perform the

following operations in the ODE solver:

$$
\begin{array}{ll}
\hat{x} = A^N_{32a} w^N(t) & , \dim \hat{x} = n_q \times 1 \\
\text{for } j = 1 : m_y + 1 & \\
\quad \hat{b} = P^\ell_j(\hat{x}) & , \dim \hat{b} = n_q \times 1 \\
\quad A^N_{32bj2}\left(w^N(t)\right) = \hat{b} * ones(1, m_x + 1) & , \dim A^N_{32bj2}\left(w^N(t)\right) = n_q \times (m_x + 1) \\
\quad A^N_{32bj}\left(w^N(t)\right) = A^N_{32bj1} \circ A^N_{32bj2}\left(w^N(t)\right) & , \dim A^N_{32bj}\left(w^N(t)\right) = n_q \times (m_x + 1) \\
\quad ind1 = (j-1) \cdot (m_x + 1) + 1 & \\
\quad ind2 = j \cdot (m_x + 1) & \\
\quad A^N_{32b}\left(w^N(t)\right)(:, ind1 : ind2) = A^N_{32bj}\left(w^N(t)\right) & , \dim A^N_{32b}\left(w^N(t)\right) = n_q \times m \\
\text{end} & \\
A^N_{32}\left(w^N(t)\right) = \rho_f A^N_{32aw} \cdot A^N_{32b}\left(w^N(t)\right) & , \dim A^N_{32}\left(w^N(t)\right) = (n-1) \times m \; .
\end{array}
$$

By creating the matrices A^N_{32a} , A^N_{32aw} and A^N_{32bj1} offline, the time needed to solve the ODE system is reduced thus improving the efficiency of the scheme for parameter estimation and control applications.

4 Parameter Estimation Problem

The goal of the parameter estimation problem is to determine the "true" material parameters $\rho_b, EI, c_D I$ and $\mathcal{K}^S_i$, $\mathcal{K}^B_i$, $i = 1, \cdots, s$, given data measurements $\hat{z}$ from some observable subspace Z of the state space. To pose this mathematically, we let $q = (\rho_b, EI, c_D I, \mathcal{K}^B_1, \cdots, \mathcal{K}^B_s, \mathcal{K}^S_1, \cdots, \mathcal{K}^S_s)$ and assume that $q \in Q$ where Q denotes an appropriately chosen admissible parameter space. The parameter estimation problem is to then seek $\bar{q} \in Q$ which minimizes

$$J(q) = \left| \mathcal{C}_2\Big[\mathcal{C}_1\left\{\mathcal{Z}(t_i, q)\right\} - \hat{z}_i\Big]\right|^2 \tag{4.3}$$

given pointwise temporal measurements $\hat{z}_i = \hat{z}(t_i)$ at given points on the beam and in the cavity. Note that this minimization is performed subject to $\mathcal{Z} = (\phi, x, \dot{\phi}, \dot{w})$ satisfying the coupled system equations (2.12) or (2.16). Depending on the experimental apparatus, the data observations may consist of position, velocity, acceleration, or accumulated strain measurements at points on the beam as well as pressure measurements inside the cavity. The form of the operator $\mathcal{C}_2$ depends upon whether one is performing the estimation procedures in the time domain or in the frequency domain. In the time domain, $\mathcal{C}_2$ is the identity whereas it is the Fourier transform for estimation in the frequency domain.

For time domain estimation with data consisting of position, velocity, or acceleration measurements at points $\bar{x}$ on the beam, the fit criterion functional to be minimized is

$$J(q) = \sum_i \left| \frac{\partial^\nu w}{\partial t^\nu}(t_i, \bar{x}; q) - \hat{z}_i \right|^2 \tag{4.4}$$

with $\nu = 0, 1$ or 2. On the other hand, if a patch with endpoints at x_1 and x_2 is used to collect accumulated strain measurements, an appropriate functional is

$$J(q) = \sum_i \left| \mathcal{K}^S \left(\frac{\partial w}{\partial x}(t_i, x_2; q) - \frac{\partial w}{\partial x}(t_i, x_1; q) \right) - \hat{z}_i \right|^2 \tag{4.5}$$

(see (2.9)). Here the data consists of the voltage measured across the patches. The patch data can also be combined with pressure measurements $\hat{p}_i$ at points $(\bar{x}, \bar{y})$ in the cavity to provide a fit criterion functional

$$J(q) = \sum_i \left\{ \left| \mathcal{K}^S \left(\frac{\partial w}{\partial x}(t_i, x_2; q) - \frac{\partial w}{\partial x}(t_i, x_1; q) \right) - \hat{z}_i \right|^2 + |\phi_t(t_i, \bar{x}, \bar{y}) - \hat{p}_i|^2 \right\} \tag{4.6}$$

which in some cases has more sensitivity than that in (4.5) which considers only strain measurements.

The above fit criteria can also be used with data that has been transformed to the frequency domain (in which case $\mathcal{C}_2$ is the Fourier transform), and this is indeed a common procedure for starting the optimization process with data in which several frequencies are excited (see the comments in the examples as well as [13, 14]). In this case, optimization is qualitatively performed in the frequency domain until frequencies match sufficiently so that the optimization routines will converge with the time domain data.

To facilitate the estimation of the material parameters ρ, EI and $c_D I$, we now make some assumptions regarding their spatial behavior. Because the beam and patches are considered to be homogeneous as well as uniform in width and thickness, it is reasonable to assume that the density, stiffness and damping parameters of the combined beam/piezoceramic patches are piecewise constant in nature (see for example, [15]). A suitable partition is then taken to be $\{x_k\} = \{0, a\} \bigcup \{\alpha_{ij}\}_{j=1,2}^{i=1,\cdots,s}$ where the $2s$ points $\{\alpha_{ij}\}$ are the endpoints of the s piezoceramic patches. Finally, we assume that these parameters have the form

$$\begin{aligned} \rho(x) &= \sum_{k=1}^{2s+1} c_k \tilde{B}_k(x) \quad , \quad c_1 = c_3 = \cdots = c_{2s+1} \\ EI(x) &= \sum_{k=1}^{2s+1} \tilde{c}_k \tilde{B}_k(x) \quad , \quad \tilde{c}_1 = \tilde{c}_3 = \cdots = \tilde{c}_{2s+1} \\ c_D I(x) &= \sum_{k=1}^{2s+1} \hat{c}_k \tilde{B}_k(x) \quad , \quad \hat{c}_1 = \hat{c}_3 = \cdots = \hat{c}_{2s+1} \end{aligned} \tag{4.7}$$

where the piecewise constant basis functions are defined by $\tilde{B}_k(x) \equiv H(x - x_{k-1}) - H(x - x_k)$. The coefficient constraints $c_1 = c_3 = \cdots = c_{2s+1}$, and so on, result from the uniformity of the beam in areas not covered by patches. Finally, we recall from the definitions (2.8) and (2.9) that the patch parameters $\mathcal{K}_1^B, \cdots, \mathcal{K}_s^B$, and $\mathcal{K}_1^S, \cdots, \mathcal{K}_s^S$ are simply constants which depend on piezoelectric properties, the geometry and size of the patch, and patch and bonding layer properties.

Although Q is finite dimensional with the above assumptions on the parameters, the minimization of the fit criteria in (4.4), (4.5) and (4.6) involves an infinite dimensional state and hence is not immediately tractable. With the Galerkin schemes of the the last section, however, corresponding minimization problems involving the state approximations can be developed and used when estimating physical parameters with these fit-to-data techniques. With w^N, ϕ_t^N and $H^N \subset V$ defined in the last section, finite dimensional functionals corresponding to those in (4.4), (4.5) and (4.6) are

$$J^N(q) = \sum_i \left| \frac{\partial^\nu w^N}{\partial t^\nu}(t_i, \bar{x}; q) - \hat{z}_i \right|^2 \quad , \ \nu = 0, 1, 2 \ , \tag{4.8}$$

$$J^N(q) = \sum_i \left| \mathcal{K}^S \left(\frac{\partial w^N}{\partial x}(t_i, x_2; q) - \frac{\partial w^N}{\partial x}(t_i, x_1; q) \right) - \hat{z}_i \right|^2 \tag{4.9}$$

and

$$J^N(q) = \sum_i \left\{ \left| \mathcal{K}^S \left(\frac{\partial w^N}{\partial x}(t_i, x_2; q) - \frac{\partial w^N}{\partial x}(t_i, x_1; q) \right) - \hat{z}_i \right|^2 + \left| \phi_t^N(t_i, \bar{x}, \bar{y}) - \hat{p}_i \right|^2 \right\} \ , \tag{4.10}$$

respectively. The approximate beam displacement w^N and acoustic pressure $\rho_f \phi_t^N$ at the various points are found by solving either the nonlinear finite dimensional system (3.1) or the system (3.2) if one is considering the linearized problem.

The following theorem taken from [16] specifies conditions under which convergence and continuous dependence (on data) of the solutions to the linearized finite dimensional parameter estimation problems involving the functionals (4.8), (4.9) and (4.10) can be expected.

Theorem 2. (Linearized System) Let Q be a compact subset of a metric space $\tilde{Q}$ with metric d and assume that $H^N \subset V$ approximates V in the sense that for each $\Phi \in V$, there exists $\Phi^N \in H^N$ such that

$$\left| \Phi - \Phi^N \right|_V \leq \varepsilon(N) \to 0 \text{ as } N \to \infty \ . \tag{4.11}$$

Furthermore, assume that $\sigma_1(q)$ and $\sigma_2(q)$ defined in (2.13) are V-elliptic, continuous, and satisfy the continuity with respect to parameter condition

$$|\sigma_i(q)(\Phi, \Psi) - \sigma_i(\tilde{q})(\Phi, \Psi)| \leq \gamma_i d(q, \tilde{q}) |\Phi|_V |\Psi|_V \quad , \text{ for } \Phi, \Psi \in V \tag{4.12}$$

for $i = 1, 2$ and $q, \tilde{q} \in Q$. Finally, assume that

$$q \mapsto (Bu + F)(t; q) \text{ is continuous from } Q \text{ to } L^2((0,T), V^*) \ . \tag{4.13}$$

For arbitrary q^N such that $q^N \to q$ in Q, one then has the convergence

$$\begin{aligned} z^N(t; q^N) &\to z(t; q) \quad \text{in } V \text{ norm} \\ z_t^N(t; q^N) &\to z_t(t; q) \quad \text{in } V \text{ norm} \end{aligned} \tag{4.14}$$

for $t > 0$. Here z and z_t are solutions to the linearized system (2.20) and z^N and z_t^N solve the corresponding linear finite dimensional system in H^N.

In our problems the admissible parameter space Q is taken to be a compact subset of the metric space $\tilde{Q} = [L_\infty(0,a)]^3 \times [\mathbb{R}^s]^2$ with elements satisfying the coefficient constraints specified in (4.7) as well as the physical constraints $\rho > 0$, $EI > 0$ and $c_D I > 0$ on $(0,a)$. In considering the remaining hypotheses, we note that the sesquilinear forms satisfy the ellipticity, continuity and parameter continuity conditions as long as damping is assumed in the region $\tilde{\Omega} \subset \Omega$ with $meas(\Omega \setminus \tilde{\Omega}) = 0$ (see (2.14) and (2.15)). Moreover, the input term $(F + Bu)(q)$ satisfies the condition (4.13). Finally, the convergence condition specified in (4.11) is satisfied as a consequence of the approximating properties of the cubic splines and Legendre polynomials in a Galerkin setting (see [6] for further details).

Hence, for the linearized problem with strong acoustic damping via $\tilde{\Omega}$, a subsequence of solutions $\bar{q}^N$ to the problems involving the minimization of the functionals (4.8) with $\nu = 0, 1$, (4.9) or (4.10) subject to (3.2) will converge to a solution $\bar{q}$ of the original problem of minimizing the functionals (4.4), (4.5) or (4.6) subject to (2.20). The convergence in the case involving the minimization of (4.8) with acceleration data does not follow directly from this theorem but can be obtained using results from the theory of analytic semigroups in a manner analogous to that used in [7].

With boundedness and Lipschitz continuity assumptions on the nonlinear coupling term $G(\mathcal{Z})$, similar results can be obtained for the nonlinear problem as summarized in the following remark.

Lemma 2. (Nonlinear Damped System) Consider the system with the nonlinear input term $Bu(t) + F(t) + G(\mathcal{Z}(t))$. If, in addition to assuming a continuity condition of the form (4.13) (with $Bu + F$ replaced by $Bu + F + G(\mathcal{Z})$), we also assume that $G(\mathcal{Z}(t))$ is continuous in t, uniformly Lipschitz continuous in $\mathcal{Z}$, and displays at most affine growth at ∞, then convergence results analogous to those summarized in Theorem 2 can be obtained for the nonlinear system.

We point out that these continuity assumptions on G were also made when discussing the well-posedness of the nonlinear system. Details concerning these conditions as well as arguments leading to the proof for the nonlinear case can be found in [5].

As indicated previously, the assumption of medium damping inside the cavity is often inappropriate in applications of interest. While we have not extended Theorem 2 to include the case in which acoustic damping is omitted or is weak, extensive numerical tests suggest that parameter convergence and continuous dependence of the parameters on data is being obtained in the same manner exhibited by the system having both strong acoustic and structural damping. This is demonstrated by the results in the following examples for the nonlinear 2-D structural acoustic system in which cavity damping is completely omitted.

5 Numerical Examples

To test the parameter estimation methodology, the general problem

$$
\begin{aligned}
&\phi_{tt} = c^2\Delta\phi \qquad (x,y) \in \Omega \ , t > 0 \ , \\
&\nabla\phi \cdot \hat{n} = 0 \qquad (x,y) \in \Gamma \ , t > 0 \ , \\
&\nabla\phi(t,x,w(t,x)) \cdot \hat{n} = \rho_f w_t(t,x) \qquad 0 < x < .6 \ , t > 0 \ , \\
&\rho w_{tt} + \frac{\partial^2}{\partial x^2}\left(EI\frac{\partial^2 w}{\partial x^2} + c_D I \frac{\partial^3 w}{\partial x^2 \partial t}\right) \\
&\qquad = -\phi_t(t,x,w(t,x)) + f(t,x) + \frac{\partial^2}{\partial x^2}\sum_{i=1}^{s} \mathcal{K}_i^B u_i(t)\chi_{pe_i}(x) \qquad \begin{array}{l} 0 < x < .6 \ , \\ t > 0 \ , \end{array} \\
&w(t,0) = \frac{\partial w}{\partial x}(t,0) = w(t,.6) = \frac{\partial w}{\partial x}(t,.6) = 0 \qquad t > 0 \ \ , \\
&\phi(0,x,y) = \phi_t(0,x,y) = w(0,x) = w_t(0,x) = 0
\end{aligned}
$$

was considered. For these examples we assumed no cavity damping and hence $d \equiv 0$, $\rho_0 = \rho_f$ throughout. The cavity was assumed to have x and y dimensions $a = .6\ m$ and $\ell = 1\ m$ with a beam at one end having length $.6\ m$, width $.1\ m$ and thickness $.005\ m$ (see Figure 3). The density and Young's modulus for regions of the beam devoid of patches were taken to be $\rho_b = 2700\ kg/m^3$ and $E = 7.1 \times 10^{10}\ N/m^2$ which yields $\rho = 1.35\, kg/m$ and $EI = 73.96\, Nm^2$ for the linear mass density and stiffness parameter (see Table 1 for a compilation of the structural parameters for the system). The Kelvin-Voigt damping parameter was chosen to be $c_D I = .001\ kg\, m^3/sec$. Finally, the values $\rho_f = 1.21\ kg/m^3$ and $c = 343\ m/sec$ were used for the atmospheric density and speed of sound.

In the examples, we consider a system in which the bounding end beam has bonded to it a centered piezoceramic patch covering 1/3 of its length as shown in Figure 3. The patch is assumed to have thickness $T = .000508\ m$ and width $b = .1\ m$ (we point out that the chosen thickness value corresponds to 20 mil which is a commercially available thickness for piezoceramic patches). The Young's modulus and density were taken to be $E_{pe} = 6.3 \times 10^{10}\ N/m^2$ and $\rho_{pe} = 7650\ kg/m^3$ which are reasonable for a patch made from G-1195 piezoceramic material.

From (2.7) and (2.8), we see that the density and stiffness coefficient in the region of the combined beam and patch (Region 2) will be greater than that of the beam (Region 1) (see Figure 3). We also assume that the damping coefficient will be slightly larger in Region 2 than Region 1.

For testing purposes, the structural parameter values in regions covered by the patches were chosen as specified in Table 1. As seen there, the constant $\mathcal{K}^B = E_{pe} b d_{31}(h + 2T_{b\ell} + T)$, which arises when modeling the actuation due to the patch, was taken to be $\mathcal{K}^B = .0067\ Nm/V$ (this latter value was obtained by assuming a bonding layer of thickness $T_{b\ell} = .0001\ m$ and taking $d_{31} = 1.9 \times 10^{-10}\ m/V$ which is the value specified for G-1195 piezoceramic material). The constant $\mathcal{K}^S$ which arises when using the patches as sensors was taken to have the value $\mathcal{K}^S = 170\ V$.

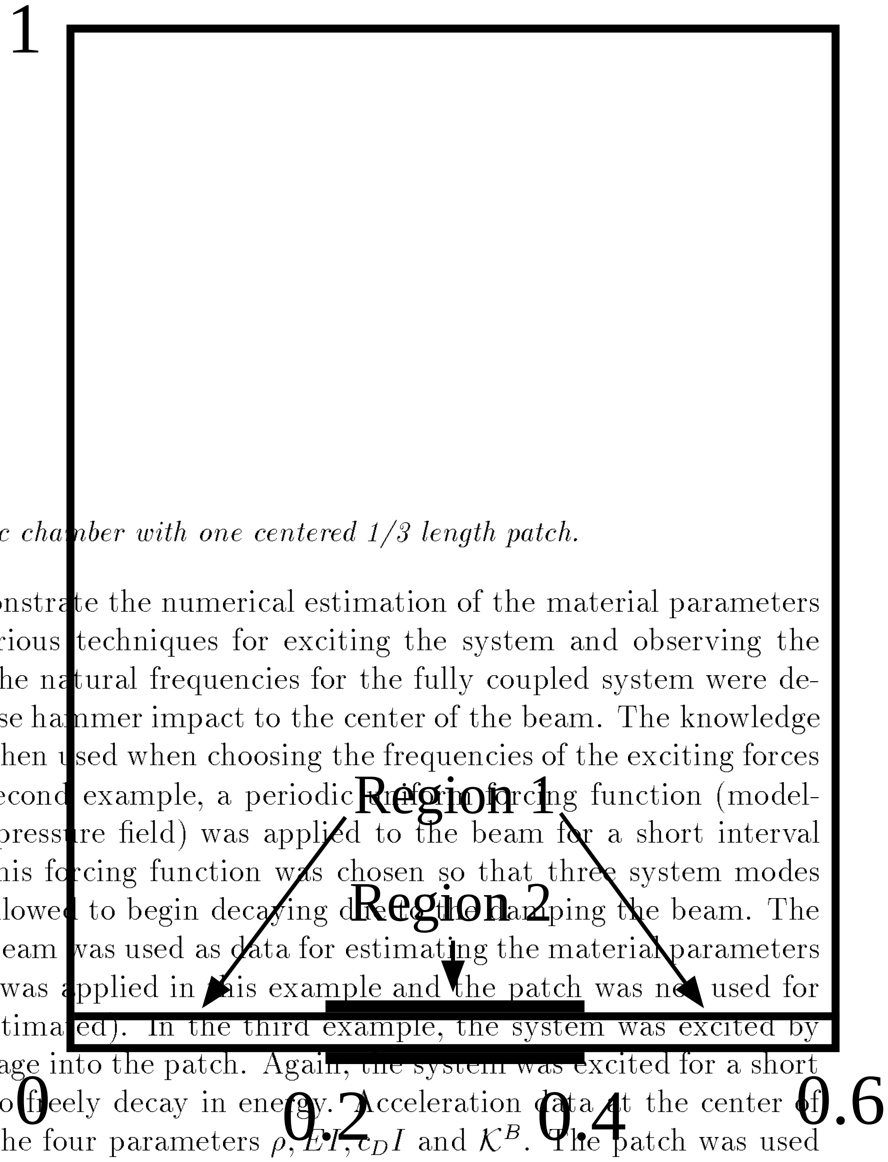

FIG. 3. *Acoustic chamber with one centered 1/3 length patch.*

The following examples demonstrate the numerical estimation of the material parameters $\rho, EI, c_D I, \mathcal{K}^B$ and $\mathcal{K}^S$ using various techniques for exciting the system and observing the response. In the first example, the natural frequencies for the fully coupled system were determined by simulating an impulse hammer impact to the center of the beam. The knowledge of these natural frequencies was then used when choosing the frequencies of the exciting forces in the other examples. In the second example, a periodic uniform forcing function (modeling a uniform exterior acoustic pressure field) was applied to the beam for a short interval of time and then set to zero. This forcing function was chosen so that three system modes were initially excited and then allowed to begin decaying due to the damping the beam. The acceleration of the center of the beam was used as data for estimating the material parameters ρ, EI and $c_D I$ (since no voltage was applied in this example and the patch was not used for sensing, $\mathcal{K}^B$ and $\mathcal{K}^S$ were not estimated). In the third example, the system was excited by the application of a periodic voltage into the patch. Again, the system was excited for a short time interval and then allowed to freely decay in energy. Acceleration data at the center of the beam was used to estimate the four parameters $\rho, EI, c_D I$ and $\mathcal{K}^B$. The patch was used both for actuating and sensing in the fourth and fifth examples. In Example 4, a periodic voltage was applied for an initial time interval after which the system energy was allowed to decay. During the decay interval, two sets of data were calculated and a comparison was made between the results obtained when each was used for recovering the parameters $\rho, EI, c_D I, \mathcal{K}^B$ and $\mathcal{K}^S$. The first data set consisted solely of the voltage produced by the patches during vibration (and hence contained strain measurements) while the second contained a combination of voltage measurements from the patch and acoustic pressure values from inside the cavity. Finally, a simulated voltage spike to the patches was used to excite the system in Example 5 (with an effect similar to that observed when an impulse hammer is used to excite the system) with the patches again being used as a sensor throughout the remainder of the time interval. Thus in the last two examples, the "smart material" aspects of the structure were utilized in determining its physical parameters.

		True Values	Initial Values (Set 1)	Initial Values (Set 2)
ρ	Region 1	1.35	1.4	1.4
(kg/m)	Region 2	2.115	2.0	2.0
EI	Region 1	73.96	74.0	75.0
(Nm^2)	Region 2	125.4	125.0	127.0
$c_D I$	Region 1	.001	.0008	.0001
$(Nm^2 sec)$	Region 2	.00125	.0008	.0001
$\mathcal{K}^B$ (Nm/V)		.0067	.007	.01
$\mathcal{K}^S$ (V)		170.0	172.0	175.0

TABLE 1. *(a) True values of the material parameters; (b) Set 1 of initial guesses for the material parameters; (c) Set 2 of initial guesses for the material parameters.*

Example 1: System Dynamics

In order to determine the system dynamics with the parameter values in Table 1, the forcing function f was chosen to simulate an impulse at the center of the beam; that is,

$$f(t,x) = \delta(x - .3)\delta(t) .$$

This models the force that would be delivered by a centered impulse hammer hit. After the initial impulse, the system was allowed to run unforced through time $T = 8/60$.

The beam acceleration obtained with $m_x = m_y = 12$ and $n = 16$ basis functions at the point $X = .3$ is plotted in Figure 4 with a corresponding frequency plot in Figure 5. The first four system responses occur at $62.9, 179.7, 342.1$ and 397.9 hertz.

For comparison, we note that the analytic natural frequencies of the first two symmetric modes of an isolated, homogeneous (no patches), undamped beam having the same dimensions as those in this system are 73.2 and 395.6 hertz while those of the uncoupled acoustic cavity are 171.5 and 343 hertz (the analytic undamped beam and cavity frequencies are given by

$$f_i = \frac{\lambda_i^2}{2\pi a^2}\sqrt{\frac{EI}{\rho}} \quad , \quad \lambda_1 = 4.7300, \lambda_2 = 7.8532, \cdots \tag{5.1}$$

and

$$f_{mn} = \frac{c}{2}\sqrt{\left(\frac{n}{a}\right)^2 + \left(\frac{m}{\ell}\right)^2} \quad , \; m = 1, \cdots \; , \; n = 0, \cdots \; ,$$

respectively). The differences between the observed and analytic values are due to the presence of the patches on the beam, the internal damping in the beam, and the coupling between the beam and acoustic field dynamics.

The frequencies observed here can also be compared with the system values 65.9, 181.3, 343.9 and 387.8 hertz which were obtained when no patches were bonded to the plate and linearized coupling conditions were assumed (see [8]). It can be seen that the increased stiffness due to the presence of the patches manifests itself at the higher frequencies (397.9 hertz versus 387.8 hertz for the uniform beam) whereas the increased density is more of a factor at the lower frequencies (62.9 hertz versus 65.9 hertz for the uniform beam). This can be explained by comparing the bending shapes of the first and third beam modes and noting that the increased stiffness is more of an influence on the third beam mode while the increased density more directly influences the first mode.

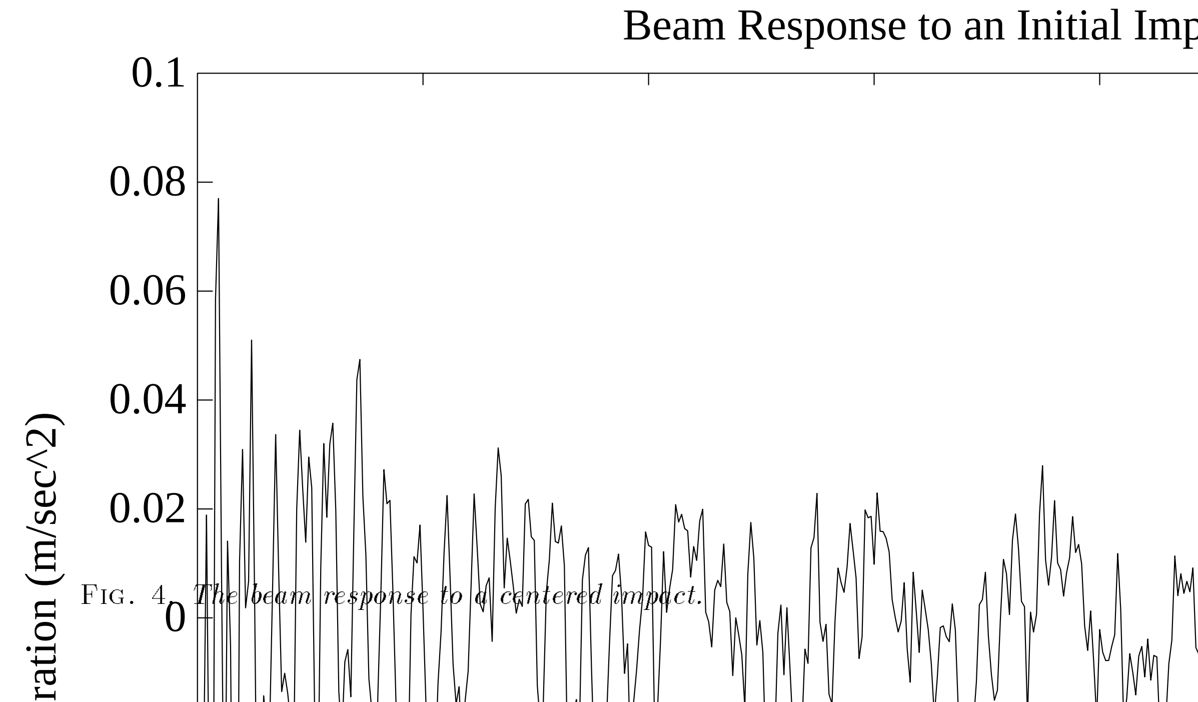

FIG. 4. *The beam response to a centered impact.*

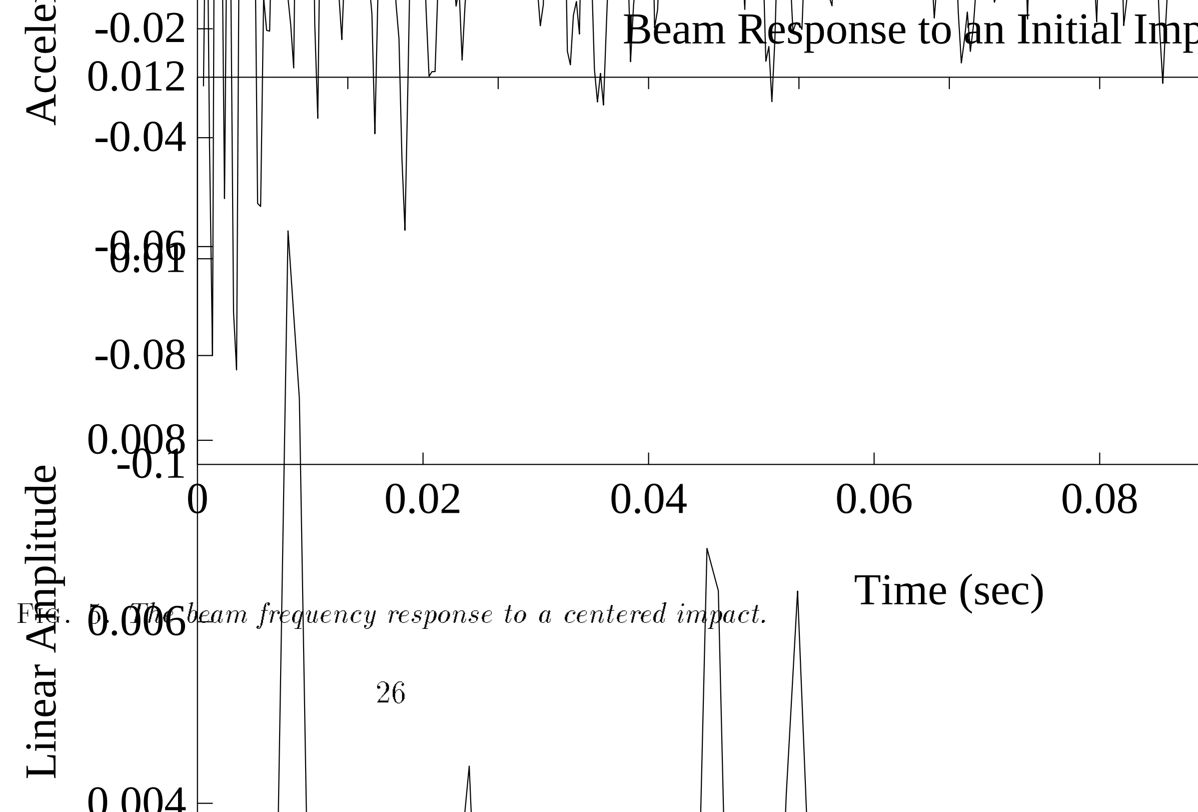

FIG. 5. *The beam frequency response to a centered impact.*

Example 2: Periodic Acoustic Excitation, Acceleration Data

In this example, a uniform (in space) periodic force modeling an acoustic plane wave was used to excite the system and acceleration data was used to estimate the parameters ρ, EI and $c_D I$ ($\mathcal{K}^B$ and $\mathcal{K}^S$ were not estimated since we were not applying voltage to the patch or using the patch for sensing). Specifically, the forcing function was taken to be

$$f(t,x) = \begin{cases} \sin(120\pi t) + \sin(360\pi t) + \sin(800\pi t) \quad , & 0 \le t \le 1/60 \\ 0 \quad , \quad 1/60 < t \le 8/60 \end{cases}$$

which initially excites the first,second and fourth system modes and then allows the oscillations to begin dying away due to the damping in the beam (see Figures 6 and 7).

The parameter estimation was performed with data which was generated by calculating the acceleration of the central point of the beam at 498 uniformly distributed points throughout the time interval $[0, 8/60]$ (hence $\nu = 2$ in (4.8)). The acceleration was determined by using a second-order central difference on the displacements which were obtained by solving the nonlinear finite dimensional system (3.1) and evaluating w^N at the points $(.3, t_k)$, $t_k = k \cdot \frac{8}{60(500)}$, $k = 2, \cdots, 499$. Due to the relatively small number of frequencies being matched, all identification procedures were performed in the time domain which implies that $\mathcal{C}_2$ in (4.3) was taken to be the identity.

To test the algorithm and software, noisefree data was first generated using 120 acoustic and 15 beam basis functions ($m_x = m_y = 10$, $n = 16$). Using the initial parameter choices in column 5 of Table 1, the parameters were estimated using the same basis choice with the optimization being performed via a Levenberg-Marquardt routine. As demonstrated by the recovered values in the third column of Table 2, very accurate estimates of the parameters can be obtained when using the same number of basis functions when generating the data and estimating the physical parameters.

To provide more realistic simulations, data was then generated using 168 acoustic and 19 beam basis functions ($m_x = m_y = 12$, $n = 20$) with 120 acoustic and 15 beam basis functions again being used for estimating the parameters (the use of a larger number of basis functions when generating the data has the effect of adding numerical noise to the values being approximated in the optimization routine). The parameter estimates obtained with noisefree data and data to which 10% relative noise was added are reported in Table 2. While these results were obtained with the initial values in column 5 of Table 1, they are representative of those obtained with a variety of initial guesses (for this method of system excitation and observation, the optimization routine converged for a relatively large range of initial values). Time and frequency domain plots of the data containing 10% noise and the acceleration obtained with the estimated parameter values of Table 2, column 5, are given in Figure 6 and 7. We note that in these figures it is essentially impossible to distinguish between the time data and the model response with estimated parameters with the graphical resolution used. These plots reinforce the observation that reasonable estimates of the parameters can be obtained with acoustic excitation and acceleration data with or without noise in the simulated data.

		No Noise (Data Set 1)	No Noise (Data Set 2)	10% Noise (Data Set 2)
ρ	Region 1	1.3500	1.3499	1.3469
(kg/m)	Region 2	2.1150	2.1149	2.1181
EI	Region 1	73.960	73.836	72.130
(Nm^2)	Region 2	125.400	125.584	130.716
$c_D I$	Region 1	.001000	.001005	.001023
$(Nm^2 sec)$	Region 2	.001250	.001232	.001091

TABLE 2. *Estimated values of ρ, EI and $c_D I$; (a) Data generated with $m_x = m_y = 10, n = 16$ and no noise added to data; (b) Data generated with $m_x = m_y = 12, n = 20$ and no noise added to data; (c) Data generated with $m_x = m_y = 12, n = 20$ and 10% noise added to the data.*

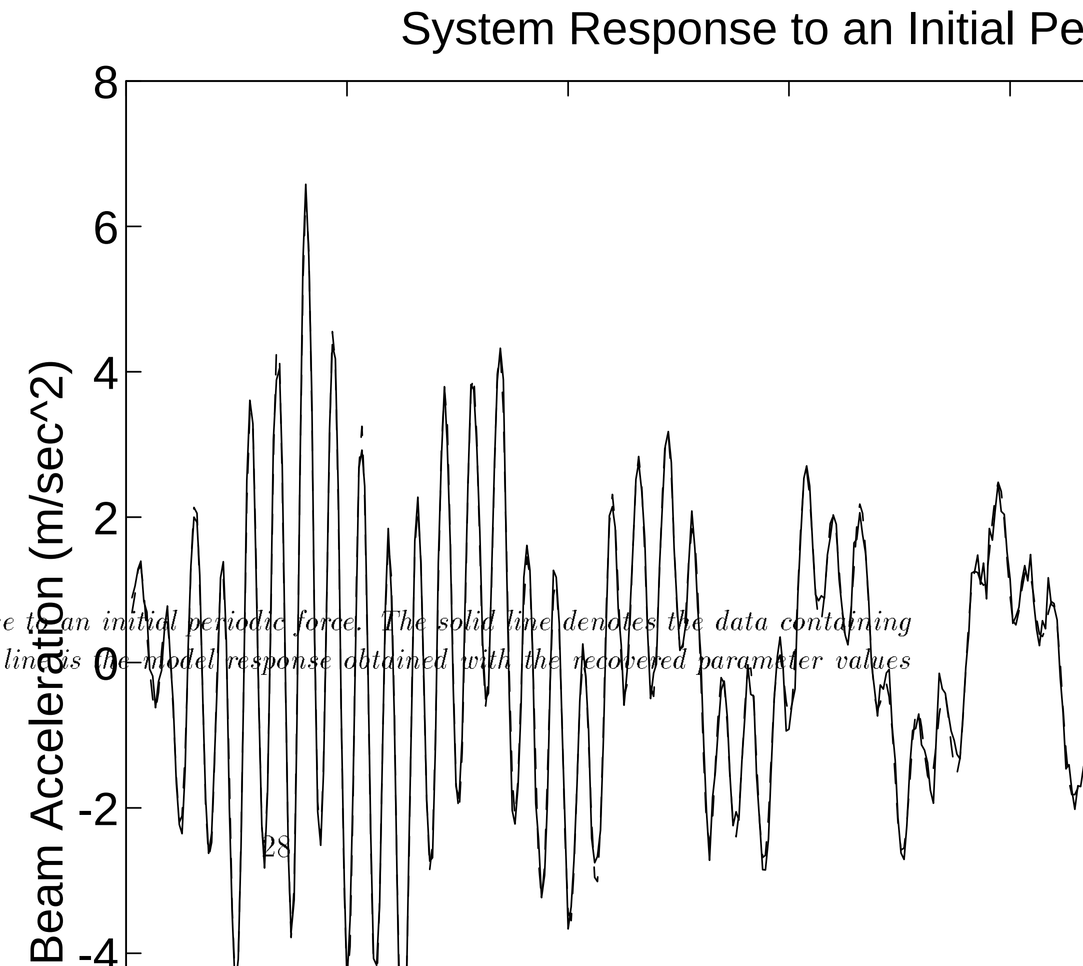

FIG. 6. *The system response to an initial periodic force. The solid line denotes the data containing 10% noise while the dashed line is the model response obtained with the recovered parameter values in column 5 of Table 2.*

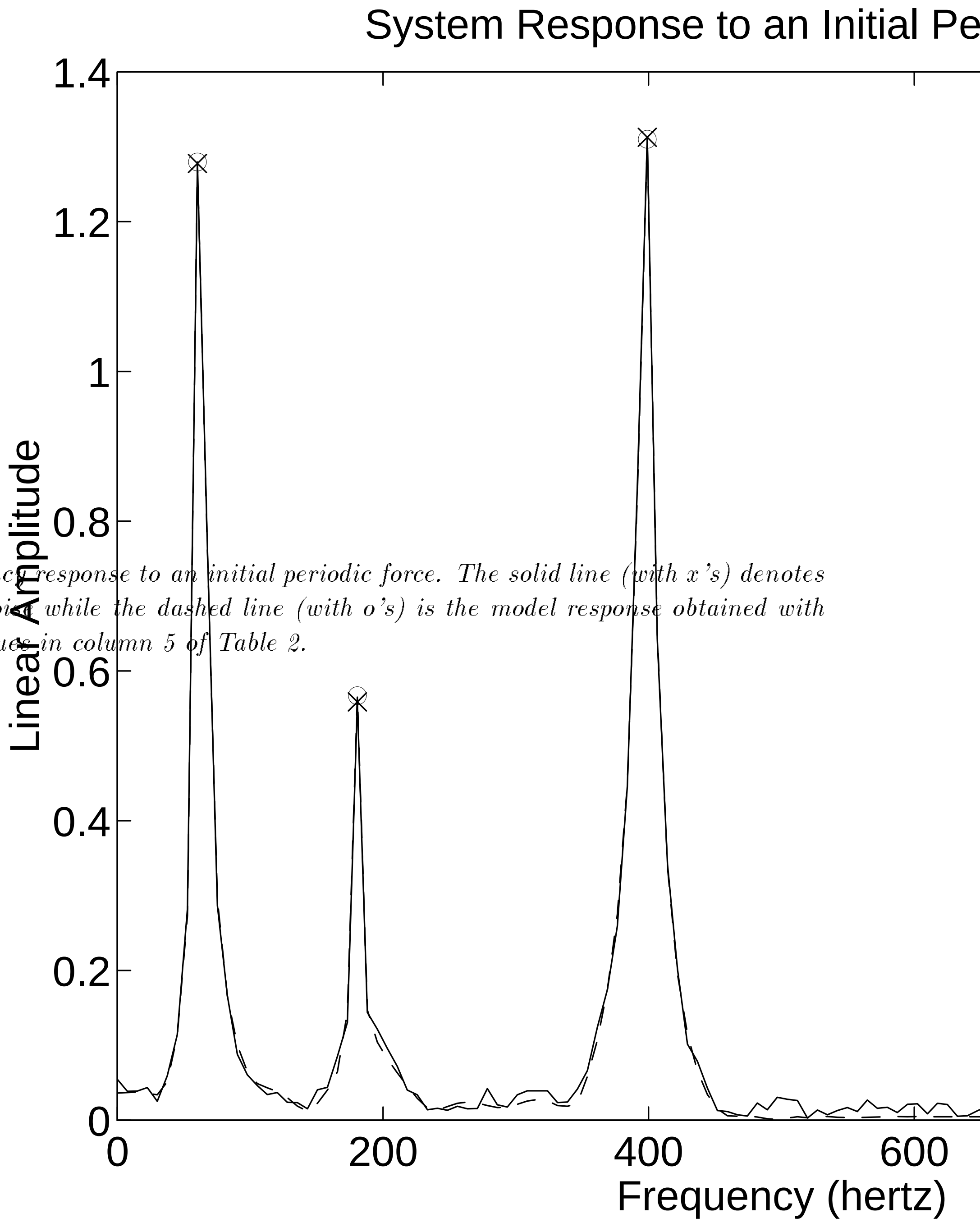

FIG. 7. *The system frequency response to an initial periodic force. The solid line (with x's) denotes the data containing* 10% *noise while the dashed line (with o's) is the model response obtained with the recovered parameter values in column 5 of Table 2.*

Example 3: Periodic Patch Excitation, Acceleration Data

A second means of exciting the system is through the application of an out-of-phase voltage to the piezoceramic patches. The driving voltage here was taken to be

$$u(t) = \begin{cases} \sin(120\pi t) + \sin(360\pi t) + (.1)\sin(800\pi t) \quad , \quad 0 \le t \le 1/60 \\ 0 \quad , \quad 1/60 < t \le 8/60 \end{cases}$$

which initially excites the first four system modes and then allows the oscillations to begin dying away due to the damping in the beam (see Figures 8 and 9). Because the patch excites the higher frequencies more efficiently than did the simulated sound field of the last example, the magnitude of the 400 hertz contribution was reduced to better balance the system response.

Acceleration data obtained in the same manner described in the last example was used to estimate the four parameters $\rho, EI, c_D I$ and $\mathcal{K}^B$ and the estimates obtained with no noise and 10% noise added to the data are summarized in Table 3 (see Table 1 for the true parameter values). Figures 8 and 9 contain the time and frequency domain results for the case in which the data contains 10% noise. In both cases, the choices $m_x = m_y = 12, n = 20$ and $m_x = m_y = 10, n = 16$ were used when generating the data and estimating parameters, respectively. Also, while similar results were obtained with a relatively large variety of starting parameter values, the parameter values reported here were obtained with the initial choices in column 3 of Table 1.

		No Noise	10% Noise
ρ	Region 1	1.3502	1.3425
(kg/m)	Region 2	2.1211	2.0973
EI	Region 1	73.139	73.449
(Nm^2)	Region 2	128.179	124.741
$c_D I$	Region 1	.000997	.000849
$(Nm^2 sec)$	Region 2	.001256	.001787
$\mathcal{K}^B$ (Nm/V)		.006771	.006654

TABLE 3. *Estimated values of $\rho, EI, c_D I$ and $\mathcal{K}^B$; (a) No noise added to the data; (b) 10% noise added to the data.*

In comparing the results obtained with noisefree data with those obtained under the same conditions (same number of basis functions and noisefree data) in the last example, we note an approximately 2% change in the estimated value of the stiffness parameter in the region covered by the patches. This difference appears to be due to the fact that the “true” data is calculated with a larger number of basis functions and hence with more accuracy than the solutions being obtained during the parameter estimation. The resulting “numerical noise” manifests itself more strongly in this case since the patches are more effective than the acoustic field at exciting high frequency oscillations which require greater accuracy to resolve (this tendency is also noted in the remaining examples where patch activation is used to excite the system). We point out that when the same number of basis functions are used for generating data and estimating parameters, the results are essentially identical to those in column 2 of Table 2 with highly accurate estimates of the physical parameters. Finally we note that the "numerical noise" due to the differing discretizations combines with random noise added to the data to simulate the noise which is present when real data is used to estimate the parameters in a physical experiment.

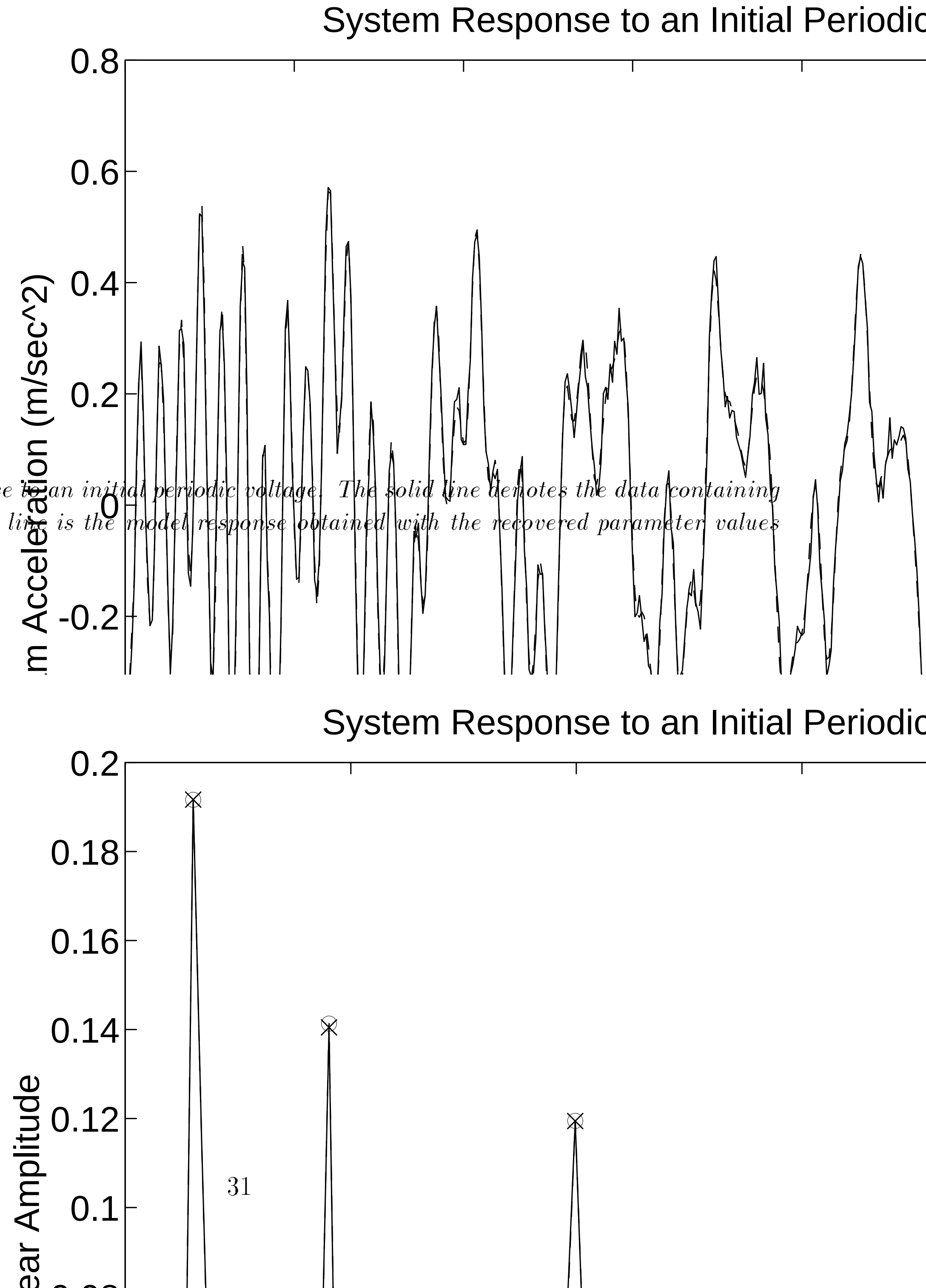

Fig. 8. *The system response to an initial periodic voltage. The solid line denotes the data containing* 10% *noise while the dashed line is the model response obtained with the recovered parameter values in Table 3.*

FIG. 9. *The system frequency response to an initial periodic voltage. The solid line (with x's) denotes the data containing* 10% *noise while the dashed line (with o's) is the model response obtained with the recovered parameter values in Table 3.*

Example 4: Periodic Patch Excitation, Patch and Pressure Data

In the previous two examples, acceleration data modeling that which would be obtained from a centered accelerometer was used in the estimation of the physical parameters. In this as well as the next example, both the excitation of the system and the sensing of the beam dynamics are performed with the patches, thus utilizing their "smart material" capabilities. The beam data in this case consists of the voltage that is produced when the patches strain during vibration (hence the criterion functional (4.9)) as well as data consisting of voltage measurements in combination with pressure measurements from within the cavity (with the criterion functional (4.10)).

Here a periodic driving voltage was applied to the patches for the first 1/5 of the time interval $[0, 10/60]$ of interest after which the system was allowed to begin decaying in energy. Specifically, the input voltage was taken to be

$$u(t) = \begin{cases} \sin(120\pi t) + \sin(360\pi t) + \sin(800\pi t) \quad , \quad 0 \le t \le 2/60 \\ 0 \quad , \quad 2/60 < t \le 10/60 \end{cases}$$

with the frequencies again chosen so as to strongly excite the first, second, fourth and sixth system modes (see Figure 5). During the final 3/4 of the time interval, the voltage produced by the patches as well as the acoustic pressure at the cavity point $(.6, .1)$ were calculated at 750 uniformly distributed times throughout the interval $[5/120, 10/60]$. These values were then used as our simulated data.

The estimated values of the parameters parameters $\rho, EI, c_D I, \mathcal{K}^B$ and $\mathcal{K}^S$ are recorded in Table 4. In the first four simulations, 168 cavity and 19 beam basis functions were used to calculate the data while 120 cavity and 15 beam basis functions were used in the estimation of the physical parameters. The values in columns 3 and 4 were obtained with data consisting of the 750 voltage values generated by the piezoceramic patches while data consisting of both voltage and acoustic pressure values was used to obtain the results in columns 5 and 6. Finally, the results from a simulation in which 120 cavity and 15 beam basis functions were used for both the generation of data and estimation of parameters are reported in column 7 of Table 4. The data for this latter simulation consisted of the previously described combination of voltage and pressure values.

It is first noted that when the same number of basis functions are used for the generation of data and estimation of parameters, highly accurate results can be obtained for a variety of initial starting values when using a combination of voltage and pressure values as data (the results in column 7 of Table 4 were obtained with the initial values in column 5, Table 1). This is consistent with the results reported in Example 2 and described in the Example 3. As discussed in the latter example, the use of a larger number of basis functions when determining the data adds a form of "numerical noise" since the data is calculated with greater accuracy than are the solutions obtained during parameter estimation. Hence, although no random noise was added to the data, the estimated values in columns 3,5 and 6 of Table 4 differ slightly from the "true" values listed in Table 1 but are consistent with those obtained in the last example (see column 3, Table 3).

The effects that the accuracy of the initial guesses had on the estimated parameters can be seen by comparing the results in columns 3 and 4 (voltage data) as well as in columns 5 and 6 (voltage and pressure data). The parameter values in columns 3 and 5 were obtained with the highly accurate initial choices of column 4, Table 1 while those in columns 4 and 6 were calculated with the less accurate values in column 5, Table 1 which could reasonably have been obtained by first visually fitting the data in the frequency domain. As observed, the change in starting values led to fairly large changes in the recovered parameter values when purely voltage data was used, whereas almost no change was noted when the data consisted of voltage and pressure values.

The variation in the recovered parameter values obtained with voltage data can partially be attributed to the flatness of the criterion functional with strain observations as compared to that seen with acceleration data. The inclusion of pressure values in the data adds richness as a result of the added information about the acoustic state as well as the fact that higher frequencies are more easily observed in the pressure data than in the stain values (see Figure 10). Due to the added information in the data containing strain and pressure values, a wider range of initial guesses could be used since the optimization routine was less like to become stuck in local minima.

		Sim1	Sim2	Sim3	Sim4	Sim5
ρ	Region 1	1.3501	1.3745	1.3502	1.3502	1.3500
(kg/m)	Region 2	2.1207	2.1476	2.1230	2.1231	2.1150
EI	Region 1	73.178	76.319	72.910	72.908	73.960
(Nm^2)	Region 2	128.022	123.546	129.041	129.051	125.400
$c_D I$	Region 1	.000992	.000283	.000989	.000988	.000999
$(Nm^2 sec)$	Region 2	.001274	.000431	.001295	.001297	.001250
$\mathcal{K}^B\ (Nm/V)$		.007274	.006709	.006767	.006766	.006700
$\mathcal{K}^S\ (V)$		158.749	85.832	172.018	171.977	169.999

TABLE 4. *Estimated values of $\rho, EI, c_D I, \mathcal{K}^B$ and $\mathcal{K}^S$; (a) Sim1: voltage data and the initial guesses of Table 1, column 5; (b) Sim2: voltage data and the initial guesses of Table 1, column 6; (c) Sim3: voltage and pressure data with the initial guesses of Table 1, column 5; (d) Sim4: voltage and pressure data with the initial guesses of Table 1, column 6; (e) Sim5: voltage and pressure data generate with same number of basis functions used in parameter estimation, initial guesses of Table 1, column 6.*

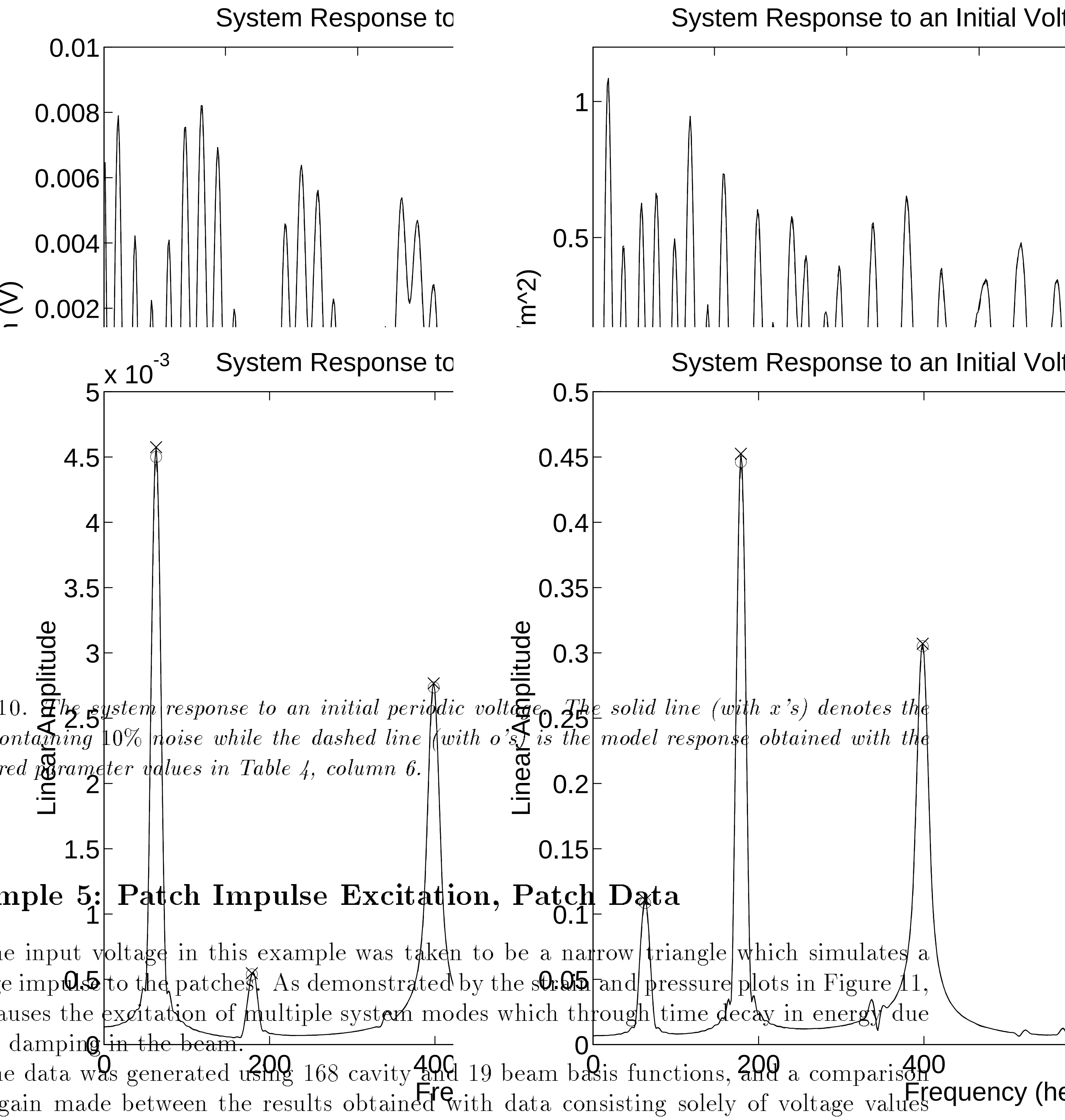

FIG. 10. *The system response to an initial periodic voltage. The solid line (with x's) denotes the data containing 10% noise while the dashed line (with o's) is the model response obtained with the recovered parameter values in Table 4, column 6.*

Example 5: Patch Impulse Excitation, Patch Data

The input voltage in this example was taken to be a narrow triangle which simulates a voltage impulse to the patches. As demonstrated by the strain and pressure plots in Figure 11, this causes the excitation of multiple system modes which through time decay in energy due to the damping in the beam.

The data was generated using 168 cavity and 19 beam basis functions, and a comparison was again made between the results obtained with data consisting solely of voltage values (using the criterion functional in (4.9)) and data made up of both voltage and pressure measurements (with the criterion functional in (4.10)). In both cases, the data was calculated at 900 uniformly spaced points throughout the time interval $[1/60, 10/60]$

The parameter values obtained with 120 cavity and 15 beam basis functions and strain (voltage values) data are given in Table 5. The initial guesses of column 5, Table 1 were used to obtain both the results containing 10% random noise and those to which no noise was added (the noisefree results can be seen to be quite close to those obtained in the last two examples). Finally, plots containing the time and frequency domain results for the case in which 10% random noise was added to the data are given in Figure 11.

We point out that with this means of system excitation, a much wider range of initial guesses led to convergence to the reported values than was the case in the last example where a periodic voltage was used to excite the system. This appears to be due to the fact that a larger number of frequencies are excited and observed in the strain data which in turn leads to "richer" data. On the other hand, the large number of frequencies observed in the pressure field (see Figure 11) made it difficult to use pressure values in combination with the voltage as data since an extremely good initial guess was required in order to obtain convergence of the optimization routine (in this case, one must work nearly exclusively in the frequency domain at first since any deviation in the density and stiffness parameters leads to frequency changes (see (5.1)) that make estimation in the time domain very difficult). We also noted that similar problems were encountered when acceleration data was used with this number of frequencies excited due to the fact that the acceleration provides a more sensitive measure of beam movement than do the patches which measure accumulated strain. Hence, with a large number of frequencies excited, the role of the patches as the sole sensors in the structural acoustic system appears to improve, and in some cases this method of data observation may be preferable since the matching of a smaller number of observed frequencies may lead to a more tractable optimization problem.

		No Noise	10% Noise
ρ	Region 1	1.3516	1.3534
(kg/m)	Region 2	2.1236	2.1218
EI	Region 1	73.261	73.969
(Nm^2)	Region 2	128.156	126.152
$c_D I$	Region 1	.000993	.000959
$(Nm^2 sec)$	Region 2	.001273	.001334
$\mathcal{K}^B\ (Nm/V)$		.006677	.006188
$\mathcal{K}^S\ (V)$		173.200	183.266

TABLE 5. *Estimated values of* $\rho, EI, c_D I, \mathcal{K}^B$ *and* $\mathcal{K}^S$ *using strain data; (a) No noise added to the data; (b)* 10% *noise added to the data.*

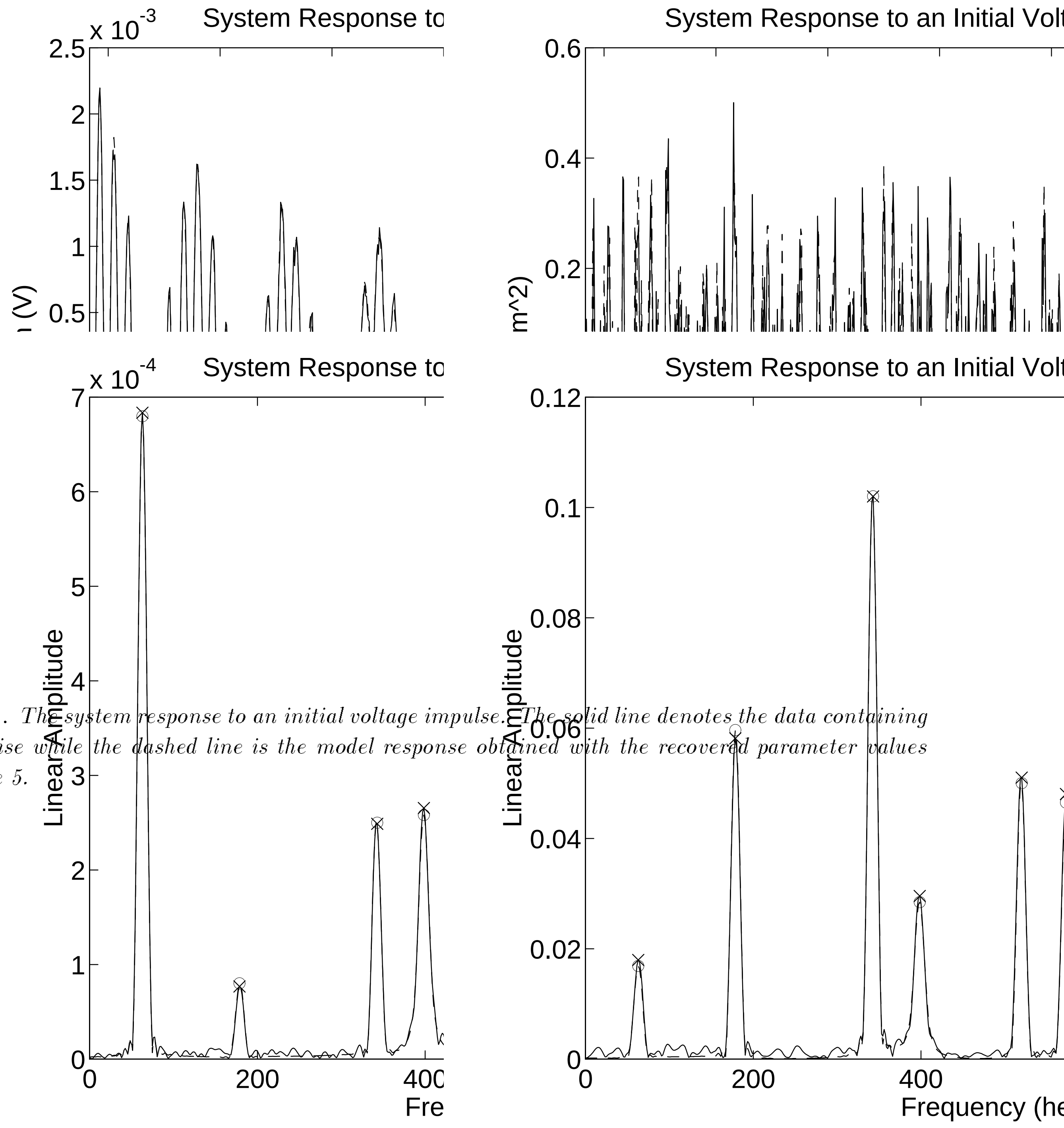

FIG. 11. *The system response to an initial voltage impulse. The solid line denotes the data containing 10% noise while the dashed line is the model response obtained with the recovered parameter values in Table 5.*

6 Conclusions and Implementation Issues

In this paper, a parameter estimation methodology for structural acoustic systems in which piezoceramic patches on the structure act as sensors and actuators has been presented. While illustrated throughout this presentation in the context of a 2-D acoustic cavity with a thin beam at one end, the methods developed here are equally applicable in many 3-D distributed parameter models (such as those in [9, 10]) of actual experimental devices currently being used to test various modeling, parameter estimation and control schemes involving piezoceramic actuators and sensors. Recently, these estimation methods have been successfully used as an integral part of feedback control techniques with experimental data - these findings will be reported in a future report.

The emphasis in developing this parameter estimation methodology was on providing a scheme which was amenable to approximation and implementation under a variety of (possibly weak) damping assumptions. In doing so, conditions leading to well-posedness and parameter convergence results for both the linearized and original nonlinear problem were discussed, and suitable numerical techniques for approximating system dynamics and implementing the parameter estimation schemes were developed.

To illustrate the method, several numerical examples illustrating a variety of techniques for exciting the system and generating data were presented. Throughout the examples, emphasis was placed on simulating exterior forces and generating data in a manner consistent with that used in actual structural acoustics experiments and applications. This was done so as to gain insight regarding the effectiveness of the parameter estimation method in various settings. The first step in the examples was the determination of the natural frequencies for the symmetric (in x) modes of the coupled system. This knowledge was then used when determining driving frequencies so as to evoke particular system responses in the later examples. Moreover, by comparing the results for the system under investigation with comparable results obtained for the structural acoustic system in which no patches were bonded to the beam as well as analytic values of the natural frequencies of the uncoupled beam and acoustic wave, the qualitative effects of coupling, damping, and material changes due to the presence of the patches were determined.

A simulated acoustic source was used to excite the beam, and hence the system, in the second example with data consisting of acceleration values calculated at the center of the beam. While the numerical simulations demonstrated the success of the method for both noisefree data and data to which random noise had been added, this means of exciting the system in a manner that can be accurately simulated will be difficult to implement. This is due to the fact that although speakers can be used to create multiple frequency acoustic forces of the type used in the example, it will be difficult, if not impossible, to cleanly cut the acoustic excitation at a given time since the speaker and room will continue to reverberate and echo even after the power is cut. This echo or reverberation will be difficult to simulate in the system model thus making parameter estimation through this means of system excitation difficult to use in practice.

A more readily simulated means of exciting the system is through the application of a prescribed voltage to the patches and this was the input in the remaining examples (by altering the frequencies and magnitude, this voltage can be tailored so as to evoke a desired system response). In the third and fourth examples, a numerically simulated multiple frequency, periodic voltage was used to initially excite the system at which point the voltage was cut and the system energy was allowed to begin decaying due to the damping in the beam. In addition to being more accurately simulated numerically, this also proved to be a more effective means of exciting high frequency responses in the system than was the acoustic excitation. A short duration triangular input was applied to the patch in the final example to simulate an initial voltage spike.

In the third example, acceleration values on the beam were used as data, whereas voltage values (measuring accumulated strain in the beam) and voltage values in combination with acoustic pressure values were used as data in the fourth and fifth examples. In these examples, it was found that when only a few system frequencies were excited (three or four), the acceleration data was sufficiently sensitive so as to permit effective parameter estimation whereas highly accurate initial guesses were needed in order to use beam data containing only strain information (which qualitatively has the properties of displacement data). By augmenting the strain data with pressure measurements, however, sufficient information was added so as to again lead to successful parameter identification with a range of initial values. On the other hand, the excitation of large number of system frequencies through the simulated voltage spike to the patch led to strain data which was sufficiently "rich" so as to permit success of the method while the introduction of pressure data led to a failure in the optimization routine due to the very large number of frequencies in the pressure measurements. Hence the success of the method with strain measurements comprising part of the data depended partly on the number of excited frequencies; for a small number, the strain measurements had to be supplemented with acceleration or pressure values in order to ensure parameter convergence for data containing any noise.

ACKNOWLEDGEMENTS: The authors would like to thank J.A. Mann, Department of Aerospace Engineering and Engineering Mechanics, Iowa State University and H.C. Lester, V.L. Metcalf and R.J. Silcox, Acoustics Division, NASA Langley Research Center for input and suggestions during several discussions concerning the modeling of the structural acoustic system being used in this work. The authors are also most grateful to Dr. Yun Wang for numerous helpful conversations and suggestions regarding the parameter estimation methods developed in this paper.

References

[1] H.T. Banks, W. Fang, R.J. Silcox and R.C. Smith, "Approximation Methods for Control of Acoustic/Structure Models with Piezoceramic Actuators," *Journal of Intelligent Material Systems and Structures,* **4**(1993), pp. 98-116.

[2] H.T. Banks and K. Ito, "A Unified Framework for Approximation in Inverse Problems for Distributed Parameter Systems," *Control-Theory and Advanced Technology* **4**(1988), pp. 73-90.

[3] H.T. Banks, K. Ito and Y. Wang, "Well-Posedness for Damped Second Order Systems with Unbounded Input Operators," Center for Research in Scientific Computation Technical Report, CRSC-TR93-10, North Carolina State University, *Differential and Integral Equations*, 8 (1995), pp. 587-606.

[4] H.T. Banks, F. Kappel and C. Wang, "Weak Solutions and Differentiability for Size Structured Population Models," in *Int. Series of Num. Math.,* Vol. 100, Birkhäuser, 1991, pp. 35-50.

[5] H.T. Banks and K. Kunisch, "An Approximation Theory for Nonlinear Partial Differential Equations with Applications to Identification and Control," *SIAM J. Control and Optimization*, **20**(1982), pp. 815-849.

[6] H.T. Banks and K. Kunisch, *Estimation Techniques for Distributed Parameter Systems,* Birkhäuser, Boston, 1989.

[7] H.T. Banks and D.A. Rebnord, "Analytic Semigroups: Applications to Inverse Problems for Flexible Structures," *Differential Equations with Applications*, (ed. by J. Goldstein, et. al.), Marcel Dekker, 1991, pp. 21-35.

[8] H.T. Banks, R.J. Silcox and R.C. Smith, "The Modeling and Control of Acoustic/Structure Interaction Problems via Piezoceramic Actuators: 2-D Numerical Examples," *ASME Journal of Vibration and Acoustics*, 116 (1994), pp. 386-396.

[9] H.T. Banks and R.C. Smith, "Modeling and Approximation of a Coupled 3-D Structural Acoustic Problem," *Computation and Control III,* Proc. Third Bozeman Conf., Bozeman, MT, 1992, Progress in Systems and Control Theory, Vol. 15, Birkhäuser Boston, Inc., 1993, pp. 29-48.

[10] H.T. Banks and R.C. Smith, "Well-Posedness of a Model for Structural Acoustic Coupling in a Cavity Enclosed by a Thin Cylindrical Shell," ICASE Report 93-10, *Journal of Mathematical Analysis and Applications*, 191 (1995), pp. 1-25.

[11] H.T. Banks and R.C. Smith, "Active Control of Acoustic Pressure Fields Using Smart Material Technologies," ICASE Rpt. No. 93-31, NASA Langley Res. Ctr.; Proceedings of the Workshop on Flow Control, Institute for Mathematics and Its Applications (IMA), University of Minnesota, Minneapolis, MN, November 16-20, 1992.

[12] H.T. Banks, R.C. Smith and Y. Wang, "Modeling Aspects for Piezoceramic Patch Activation of Shells, Plates and Beams," Center for Research in Scientific Computation Technical Report, CRSC-TR92-12, North Carolina State University; *Quarterly of Applied Mathematics*, to appear.

[13] H.T. Banks and Y. Wang, "Parameter Identification in the Frequency Domain," *Computation and Control III,* Proc. Third Bozeman Conf., Bozeman, MT, 1992, Progress in Systems and Control Theory, Vol. 15, Birkhäuser Boston, Inc., 1993, pp. 49-62.

[14] H.T. Banks, Y. Wang and D.J. Inman, "Bending and Shear Damping in Beams: Frequency Domain Estimation Techniques," *Journal of Vibration and Acoustics*, 116 (1994), pp. 188-197.

[15] H.T. Banks, Y. Wang, D.J. Inman and J.C. Slater, "Variable Coefficient Distributed Parameter System Models for Structures with Piezoceramic Actuators and Sensors," Proc. of the 31^{st} Conf. on Decision and Control, Tucson, AZ, Dec. 16-18, 1992, pp. 1803-1808.

[16] H.T. Banks, Y. Wang, D.J. Inman and J.C. Slater, "Approximation and Parameter Identification for Damped Second Order Systems with Unbounded Input Operators," Center for Research in Scientific Computation Technical Report, CRSC-TR93-9, North Carolina State University, *Control: Theory and Advanced Technology*, 10 (1994), pp. 873-892.

[17] G. Da Prato, "Synthesis of Optimal Control for an Infinite Dimensional Periodic Problem," *SIAM J. Control Opt.*, **25**(1987), pp. 706-714.

[18] J.J. Dosch, D.J. Inman and E. Garcia, "A Self-Sensing Piezoelectric Actuator for Collocated Control," *Journal of Intelligent Material Systems and Structures,* **3**(1992), pp. 166-185.

[19] A. Haraux, "Linear Semigroups in Banach Spaces," in *Semigroups, Theory and Applications, II* (H. Brezis, et al., eds.), Pitman Res. Notes in Math, Vol 152, Longman, London, 1986, pp. 93-135.

[20] M.P. Norton, *Fundamentals of Noise and Vibration Analysis for Engineers*, Cambridge University Press, New York, 1989.

[21] A. Pazy, *Semigroups of Linear Operators and Applications to Partial Differential Equations,* Springer-Verlag, New York, 1983.

[22] J. Wloka, *Partial Differential Equations*, Cambridge University Press, New York, 1987.